nature methods

ARTICLES

https://doi.org/10.1038/s41592-019-0404-0

SABER amplifies FISH: enhanced multiplexed imaging of RNA and DNA in cells and tissues

Jocelyn Y. Kishi[1,2,6], Sylvain W. Lapan[3,6], Brian J. Beliveau[1,2,5,6*], Emma R. West[3,6], Allen Zhu[1,2], Hiroshi M. Sasaki[1,2], Sinem K. Saka[1,2], Yu Wang[1,2], Constance L. Cepko[3,4*] and Peng Yin[1,2*]

Fluorescence in situ hybridization (FISH) reveals the abundance and positioning of nucleic acid sequences in fixed samples. Despite recent advances in multiplexed amplification of FISH signals, it remains challenging to achieve high levels of simultaneous amplification and sequential detection with high sampling efficiency and simple workflows. Here we introduce signal amplification by exchange reaction (SABER), which endows oligonucleotide-based FISH probes with long, single-stranded DNA concatemers that aggregate a multitude of short complementary fluorescent imager strands. We show that SABER amplified RNA and DNA FISH signals (5- to 450-fold) in fixed cells and tissues. We also applied 17 orthogonal amplifiers against chromosomal targets simultaneously and detected mRNAs with high efficiency. We then used 10-plex SABER-FISH to identify in vivo introduced enhancers with cell-type-specific activity in the mouse retina. SABER represents a simple and versatile molecular toolkit for rapid and cost-effective multiplexed imaging of nucleic acid targets.

FISH allows researchers to interrogate the subcellular distribution of RNA and DNA molecules in fixed cells and tissues through the application of complementary probes[1]. FISH assays are used for diverse applications such as diagnosing chromosomal abnormalities[2], interrogating three-dimensional (3D) genome organization[3] and analyzing gene expression[4,5]. FISH is compatible with simultaneous detection of multiple nucleic acid targets, and when it is combined with sequential imaging methods, the number of detectable targets can be greater than the number of spectrally resolvable fluorophores[3,6,7]. Recent approaches that utilize serial rounds of imaging, label removal and relabeling of distinct targets enable researchers to image potentially unlimited numbers of targets. For example, techniques such as DNA-Exchange[8–10], which uses cyclic rounds of hybridization and displacement of fluorescently labeled oligonucleotides bound to probes, can be used to visualize a large number of targets (up to 84 distinct chromosomal regions in cultured cells[11,12] and 33 RNA transcripts in tissues[13]). For higher levels of multiplexing, multiple-round combinatorial labeling allows a linear number of serial imaging rounds to visualize an exponential number of low-abundance targets, provided that the targets are optically resolvable[14–17].

Beyond multiplexing, several approaches have been developed to amplify the intensity of quantitative FISH signals. Amplification is particularly relevant in the context of thick tissues, where high levels of autofluorescence, light scattering and optical aberration can make signal detection challenging. In addition, amplification of signal can shorten imaging times (increasing throughput), further reduce requirements for expensive microscopy setups and potentially reduce costs by decreasing the number of probes required. Previous amplification strategies have included the targeted deposition of detectable reactive molecules around the site of probe hybridization[18]; the targeted assembly of 'branched' structures composed of DNA[19,20] or locked nucleic acid molecules[21]; the programmed in situ growth of concatemers by enzymatic rolling-circle amplification (RCA)[22] or hybridization chain reaction (HCR)[23–26]; and the assembly of topologically catenated DNA structures using serial rounds of chemical ligation[27].

Amplification methods that utilize simultaneous orthogonal amplification, such as HCR and RCA, enable efficient multiplexed visualization of targets in tissue. HCR uses triggered self-assembly of pairs of self-folding hairpin oligonucleotides into long concatemeric chains to achieve simultaneous enzyme-free amplification in situ. However, to date, only five orthogonal HCR concatemers have been demonstrated; this is potentially due to the complexity of designing multiple complex, non-interacting kinetic pathways of triggered autonomous hairpin assembly that are able to operate simultaneously. RCA-based approaches have been used to simultaneously amplify eight target mRNAs in mouse lung tissue[28], and to detect up to 28 mRNA targets simultaneously in cleared 150-µm mouse tissue sections and up to 1,020 spatially separated targets in thin (single-cell-layer) sections[29]. While RCA-based methods enable highly multiplexed simultaneous amplification, detection efficiencies for RNA transcripts remain comparable to those in single-cell RNA sequencing (6–40%) in the best case (STARmap) and are also low for other RCA-based methods such as FISSEQ (0.01–0.2%) and designs that are based on padlock probes (5–32%)[28,29], perhaps owing to the complexity of controlling parallel enzymatic reactions in situ.

Here we sought to develop an amplification method with (1) programmable and high levels of amplification, (2) high orthogonality to allow simultaneous amplification and (3) high targeting efficiency, including in thick tissues. In addition to these performance characteristics, we further desired the method to be accessible, utilizing (4) a simple and robust workflow compatible with commonly available imaging platforms and (5) cost-effective and readily available reagents.

We developed an amplification method to meet these performance and accessibility criteria by using a programmable

[1]Wyss Institute for Biologically Inspired Engineering, Harvard University, Boston, MA, USA. [2]Department of Systems Biology, Harvard Medical School, Boston, MA, USA. [3]Department of Genetics, Blavatnik Institute, Harvard Medical School, Boston, MA, USA. [4]Howard Hughes Medical Institute, Chevy Chase, MD, USA. [5]Present address: Department of Genome Sciences, University of Washington, Seattle, WA, USA. [6]These authors contributed equally: Jocelyn Y. Kishi, Sylvain W. Lapan, Brian J. Beliveau, Emma R. West. *e-mail: beliveau@uw.edu; cepko@genetics.med.harvard.edu; py@hms.harvard.edu

single-stranded (ssDNA) synthesis method that we recently developed, the primer-exchange reaction (PER)[30]. We previously demonstrated the growth of long ssDNA concatemers composed of a three-letter code of A, T and C nucleotides from a short (9-nucleotide) DNA primer sequence with PER[30]. We found that the kinetics of the synthesis reaction are controllable via a number of parameters, providing a simple means of generating concatemers of the desired length through in vitro synthesis. Here we show that these concatemers permit amplification of fluorescent signal, as their polymeric structure provides a hybridization scaffold for localizing many fluorescent imager oligonucleotides, reminiscent of the sequences found in branched approaches to signal amplification[19–21]. PER can also be used to synthesize a large number of orthogonal concatemer sequences, and we are able to readily implement multiplexed imaging strategies with cyclic serial readout of the concatemers through the hybridization and displacement of imagers (DNA-Exchange)[8–10]. We further establish that these concatemers, which are designed to have little secondary structure, effectively penetrate thick tissue.

The molecular toolkit (SABER) harnesses the programmability, orthogonality and simplicity of PER to enhance the functionality of oligonucleotide-based FISH probes, such as single-molecule RNA FISH probe pools[5] and highly complex 'Oligopaint' probe sets[31]. In brief, DNA and RNA FISH probes are first chemically synthesized with primer sequences on their 3′ ends, which are extended into PER concatemers in vitro. The approximately 1- to 3-h PER reaction uses a set of widely available and inexpensive reagents similar to those used in PCR. Extended probe sequences are hybridized to targets in situ and then detected by secondary hybridization of fluorescent imagers, with the options of including intermediate branching concatemers for additional signal amplification or applying serial imaging with DNA-Exchange[8–10] (Exchange-SABER). In comparison with methods that generate concatemers in situ, this approach allows bulk probe production, quality control and user-defined adjustment of probe concentration.

We experimentally demonstrate that, in different scenarios, SABER can programmably amplify a signal up to 450-fold, can be deployed against 17 different targets simultaneously and can provide high sampling efficiency of target transcripts for puncta detection and cell-type identification in tissue. In a 10-plex FISH assay, we applied SABER to interrogate the activity and specificity of candidate enhancer elements introduced in vivo via the detection of reporter RNAs and markers of retinal cell types, and we show that reporter RNAs and the plasmids from which they are expressed can be simultaneously detected in a combined RNA/DNA FISH experiment. The straightforward probe synthesis and hybridization protocols, along with compatibility with common microscopes, make this method readily adoptable.

Results

Design of orthogonal sequences for SABER. We recently developed the PER method for autonomously synthesizing arbitrary ssDNA sequences from short DNA primers[30]. One version of the reaction uses a catalytic hairpin paired with a strand-displacing polymerase and competitive branch migration[32] to repeatedly add the same sequence domain onto single-stranded primers (Fig. 1a and Supplementary Fig. 1a). Representative reactant and concatemer sequences are depicted in Supplementary Fig. 1b and Supplementary Fig. 1c, respectively. We found that we could tune the length of PER concatemers by varying the concentration of polymerase, hairpin, magnesium or nucleotides, as well as the extension time (Fig. 1b and Supplementary Fig. 1d). These concatemers lack G bases to minimize secondary structure and permit GC pairs to be used as a polymerase terminator sequence within the hairpin in the absence of dGTP in the reaction. We reasoned that the PER-based concatemerization could provide a flexible means to endow FISH probes with repetitive extensions for depositing fluorescent signal. The workflow for SABER is depicted in Fig. 1c. PER concatemers are extended on chemically synthesized probes bearing a 9-nucleotide primer. After hybridization of extended probes, concatemers are detected by secondary hybridization with imager oligonucleotides (Supplementary Fig. 1e). A modular variant of SABER uses 42-nucleotide 'bridge' sequences to hybridize concatemer strands onto shorter, target-binding probes, and this can be deployed in a single hybridization incubation (Fig. 1d and Supplementary Fig. 1f). With either detection scheme, imager oligonucleotides can be stripped from their cognate concatemers to reset the signal[8–10], enabling subsequent use of that fluorescence color on a distinct target. With this Exchange-SABER approach, a multitude of PER-concatemerized probe sets can be hybridized to their targets simultaneously and read out in sequential rounds of imaging (Fig. 1e).

Sequence orthogonality was considered in all aspects of the design to ensure robust and specific targeting of fluorescent signal with multiplexed SABER. We used the OligoMiner pipeline[33] to computationally design orthogonal Oligopaint probe sequences with homology to targets of interest. The pipeline vets sequences for orthogonality against the relevant target genome, and constraints on single strandedness and melting temperature are used to further filter sequences. FISH probes are hybridized under conditions close to their melting temperature to increase the specificity of binding (Supplementary Fig. 1g). A similar design process, but with sequences drawn from blocks of orthogonal sequences[34], was used to generate 84 orthogonal 42-nucleotide bridge sequences. To successfully deploy a large number of orthogonal concatemers simultaneously using SABER, we also needed to design many orthogonal PER concatemer sequences. We used NUPACK[35–37] to model on- and off-target interactions for sets of 50 probes, fifty 42-nucleotide bridges and 50 computationally designed PER sequences in their respective incubation conditions (2× SSCT with 50% formamide at 42 °C for in situ hybridization (ISH) and 1× PBS at 37 °C for fluorescent hybridization; see Supplementary Fig. 1h). Dimerization probabilities for these sets of sequences were also modeled (Supplementary Fig. 1i).

SABER effectively amplifies fluorescent signals. We applied SABER to DNA and RNA targets with known distributions in cell culture samples. First, a DNA oligonucleotide with homology to the human telomere sequence was extended to five different lengths (conditions E1–E5) using varied concentrations of hairpin (Supplementary Fig. 2a). The fluorescence resulting from hybridization with probes of each length, and a probe with an unextended sequence with a single binding site for imagers (condition U), was visualized by fluorescence microscopy (Fig. 2a and Supplementary Fig. 2b). A custom CellProfiler[38] pipeline was used to identify and quantify puncta within cell nuclei (Supplementary Fig. 2c). We measured distributions of peak fluorescence values for puncta for all conditions (Fig. 2b, top), and we estimated fold enhancement in fluorescence by subtracting background and dividing by the mean for the unextended condition (Fig. 2b, bottom). We estimated 6.2-, 5.0-, 8.6-, 6.8- and 13.3-fold enhancement, respectively, for conditions E1 through E5 relative to the unextended (that is, unamplified) probe. See Supplementary Fig. 2d for additional analyses.

Next, the process was repeated for a set of 122 probes designed to target the mouse *Cbx5* mRNA transcript. Here, for technical utility, we used a large probe set to ensure that unamplified signal could be robustly visualized and quantified. The probes were pooled, extended to five lengths (Supplementary Fig. 2e) and visualized (Fig. 2c and Supplementary Fig. 2f). Puncta within cell bodies were segmented for analysis (Fig. 2d and Supplementary Fig. 2g). The first four extension lengths showed increasing levels of amplification (5.9-, 8.2-, 8.6- and 10.2-fold enhancement for conditions E1–E4), but the longest extension (condition E5) showed a drop-off (7.3-fold enhancement), indicating the importance

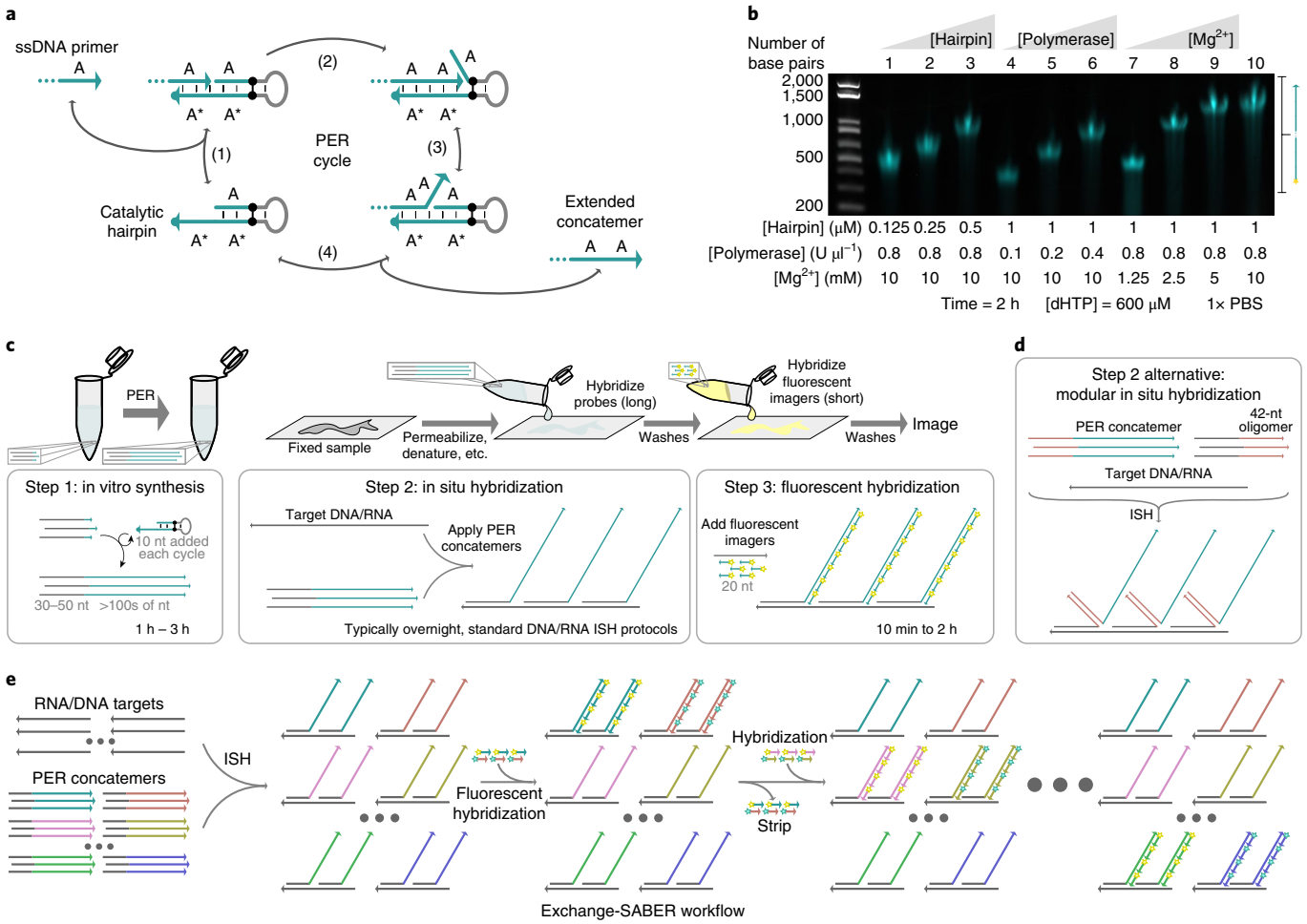

Fig. 1 | SABER-FISH design and workflow. a, PER cycle[30]. A primer with domain **A** on its 3′ end binds (reversibly) to a catalytic hairpin and is extended with a new **A** domain by a strand-displacing polymerase. **b**, Length programmability of PER concatemers by modulation of hairpin concentration, polymerase concentration, magnesium concentration and incubation time. See also Supplementary Fig. 1d. **c**, SABER workflow. First, large batches of probe sequences with primers on their 3′ ends can be concatemerized using PER. These extensions are then hybridized to DNA and RNA targets in fixed samples following standard ISH protocols. This is followed by a short step that hybridizes fluorescently labeled oligonucleotides (imagers) to complementary concatemers. **d**, An alternative method uses 42-nucleotide bridge sequences to couple probes to concatemer sequences. **e**, Exchange-SABER workflow. Optionally, fluorescent signal can be rapidly stripped from concatemers without disruption of probe binding, allowing exchange of imagers[8–10].

of the extension-length programmability available through modulation of the parameters described above. In general, our results indicate that extension lengths between ~250 and 750 nucleotides provide robust, although not substantially different, levels of amplification.

Multiple rounds of PER concatemer hybridization can further increase levels of fluorescent signal by creating branched concatemeric structures[19–21] (Supplementary Fig. 3a). A secondary round of hybridization binds PER concatemers with 30 nucleotides of homology to the primary probe concatemer. With a similar pipeline, branching amplification was visualized and quantified for several branch concatemer lengths targeting *Cbx5* mRNA transcripts (Supplementary Fig. 3b). Using this strategy, we observed up to 35.5-fold enhancement of amplification levels (Supplementary Fig. 3c and additional analyses in Supplementary Fig. 3d). Multiple rounds of branching can result in even higher levels of amplification. We implemented one to four rounds of branching (conditions B1–B4; Fig. 2e) on top of probe concatemers targeting the *Cbx5* mRNA transcript (Fig. 2f). After feature segmentation, maximum pixel values within identified puncta were quantified only under exposure times where puncta could be reliably identified (Fig. 2g and Supplementary Fig. 3e). In total, fold enhancement of signal was estimated to be 32.2-, 85.7-, 144.1- and 464.7-fold for one, two, three and four levels of branching, respectively.

SABER enables robust transcript detection in tissue. We next asked whether SABER could be used to amplify RNA FISH signal in tissue sections. The transcriptome of the mouse retina has been extensively characterized using single-cell RNA sequencing (scRNA-seq)[39,40], providing a useful point of comparison to assess the target specificity and quantifiability of FISH using SABER probes. We first compared unextended probes with PER-extended probes by targeting rhodopsin (*Rho*), expressed exclusively in rod photoreceptors (Fig. 3a). Here an exceptionally abundant mRNA was selected to permit visualization of unamplified signal in tissue sections. Fluorescent signal was localized to the photoreceptor layer (Fig. 3b), and we observed 5.2-, 6.4-, 7.0- and 7.9-fold enhancement for increasing extension lengths (E1–E4) versus unextended probes (Fig. 3c and signal-to-noise ratio (SNR) analysis in Supplementary Fig. 4a). Formaldehyde-fixed cryosections cut to a thickness of 35–40 μm were used for these and subsequent experiments.

We next tested the performance of SABER in the detection of lower-abundance transcripts, choosing rod bipolar cells (RBCs),

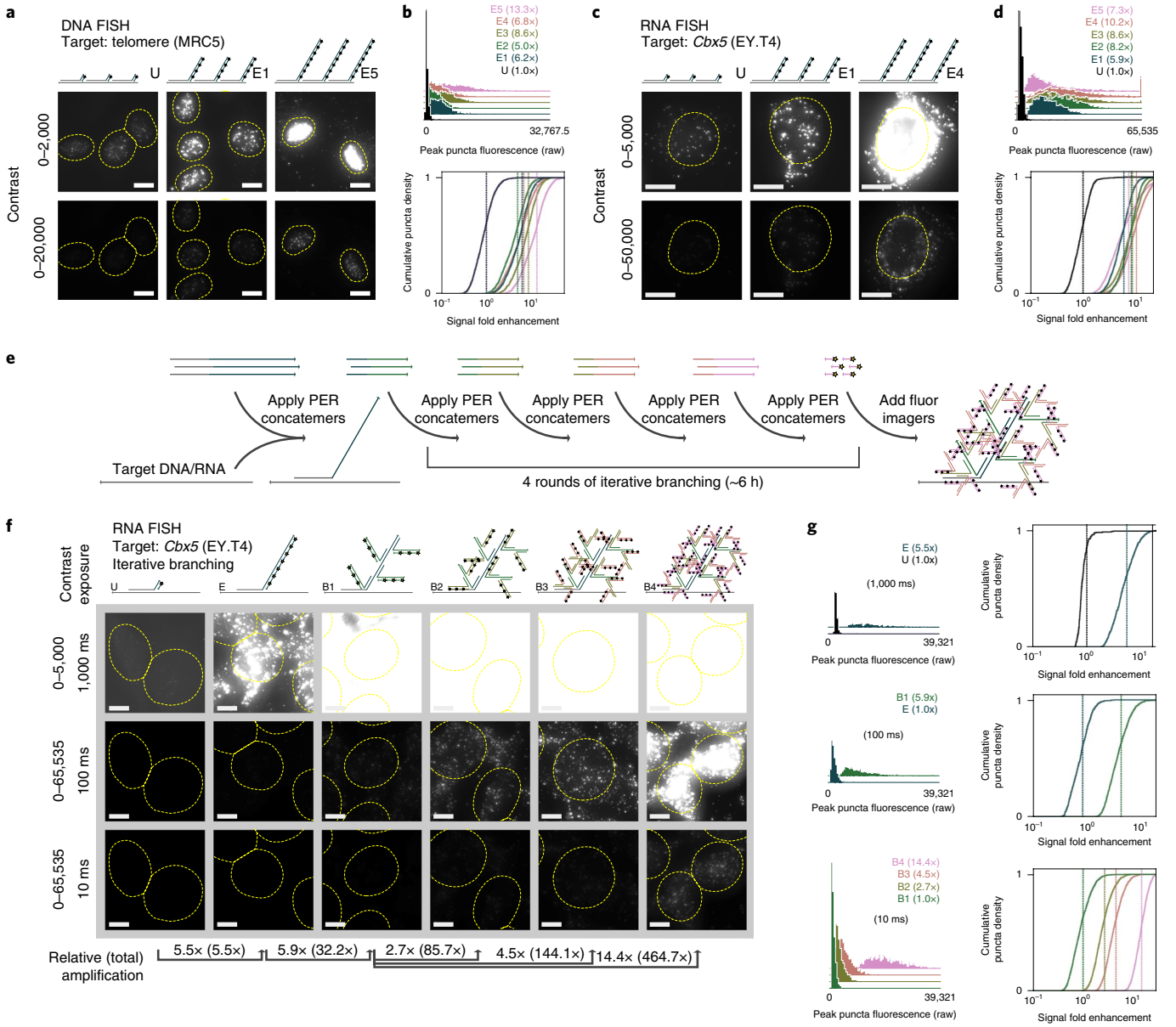

Fig. 2 | SABER effectively amplifies fluorescent signals. a, Microscopy images for the unextended PER-concatemerized probe (U) and two different lengths of PER-concatemerized probes (E1 and E5) targeting the human telomere sequence. See Supplementary Fig. 2b for images of E2, E3 and E4. **b**, Distributions of peak fluorescence values for puncta detected using CellProfiler[38] (top; fold enhancements are shown in the legend). Normalized background-subtracted cumulative distribution functions show fold enhancement over the unextended condition, with vertical lines depicting means (fold enhancement; bottom). See Supplementary Fig. 2d for additional analyses. $n_{(puncta)}$: $n_{(U)}=1{,}895$; $n_{(E1)}=1{,}846$; $n_{(E2)}=1{,}876$; $n_{(E3)}=2{,}011$; $n_{(E4)}=2{,}190$; $n_{(E5)}=2{,}006$. **c**, Images for unextended probe and two extension lengths (E1 and E4) of a 122-probe pool targeting the mouse *Cbx5* mRNA transcript. See Supplementary Fig. 2f for additional images. **d**, Distributions analogous to **b** from puncta identified within cell bodies using CellProfiler[38]. Lines corresponding to the mean are shown on the distributions. See Supplementary Fig. 2g for additional analyses. $n_{(puncta)}$: $n_{(U)}=1{,}720$; $n_{(E1)}=1{,}588$; $n_{(E2)}=1{,}649$; $n_{(E3)}=2{,}099$; $n_{(E4)}=2{,}884$; $n_{(E5)}=3{,}279$. **e**, Schematic showing how multiple rounds of PER concatemer binding (branching) can be used to further increase signal. **f**, Representative images for samples with unextended probes, extended probes and up to four rounds of branching (B1–B4) are shown. **g**, Relative fluorescence was compared as before but with no background subtraction to estimate fold enhancement in amplification. In total, fold enhancement in amplification over unextended probes was estimated to be 465-fold. Lines corresponding to the mean are shown on the distributions. See Supplementary Fig. 3e for additional analyses. $n_{(puncta,\ exposure\ time)}$: $n_{(U,\ 1{,}000\ ms)}=262$; $n_{(E,\ 1{,}000\ ms)}=928$; $n_{(E,\ 100\ ms)}=717$; $n_{(B1,\ 100\ ms)}=1{,}821$; $n_{(B1,\ 10\ ms)}=1{,}818$; $n_{(B2,\ 10\ ms)}=1{,}796$; $n_{(B3,\ 10\ ms)}=2{,}059$; $n_{(B4,\ 10\ ms)}=1{,}344$. Scale bars, 10 µm.

a single type of bipolar interneuron that has been extensively profiled by scRNA-seq[39,40], as a test population. Specificity of FISH was confirmed by simultaneous detection of the *Prkca* transcript and PRKCA protein, an established RBC marker (Fig. 3d and Supplementary Fig. 4b). As the ability to quantify detected transcripts per cell is important to assess the performance of SABER, we sought a generalizable and unbiased method for defining cell boundaries. We found that fluorophore-conjugated wheat germ agglutinin (WGA) effectively outlined retinal cells (Fig. 3e), enabling 3D cell segmentation using ACME[41], an open-source software package for membrane-based watershed segmentation (Fig. 3f). A Laplacian of Gaussian method was used to localize fluorescent

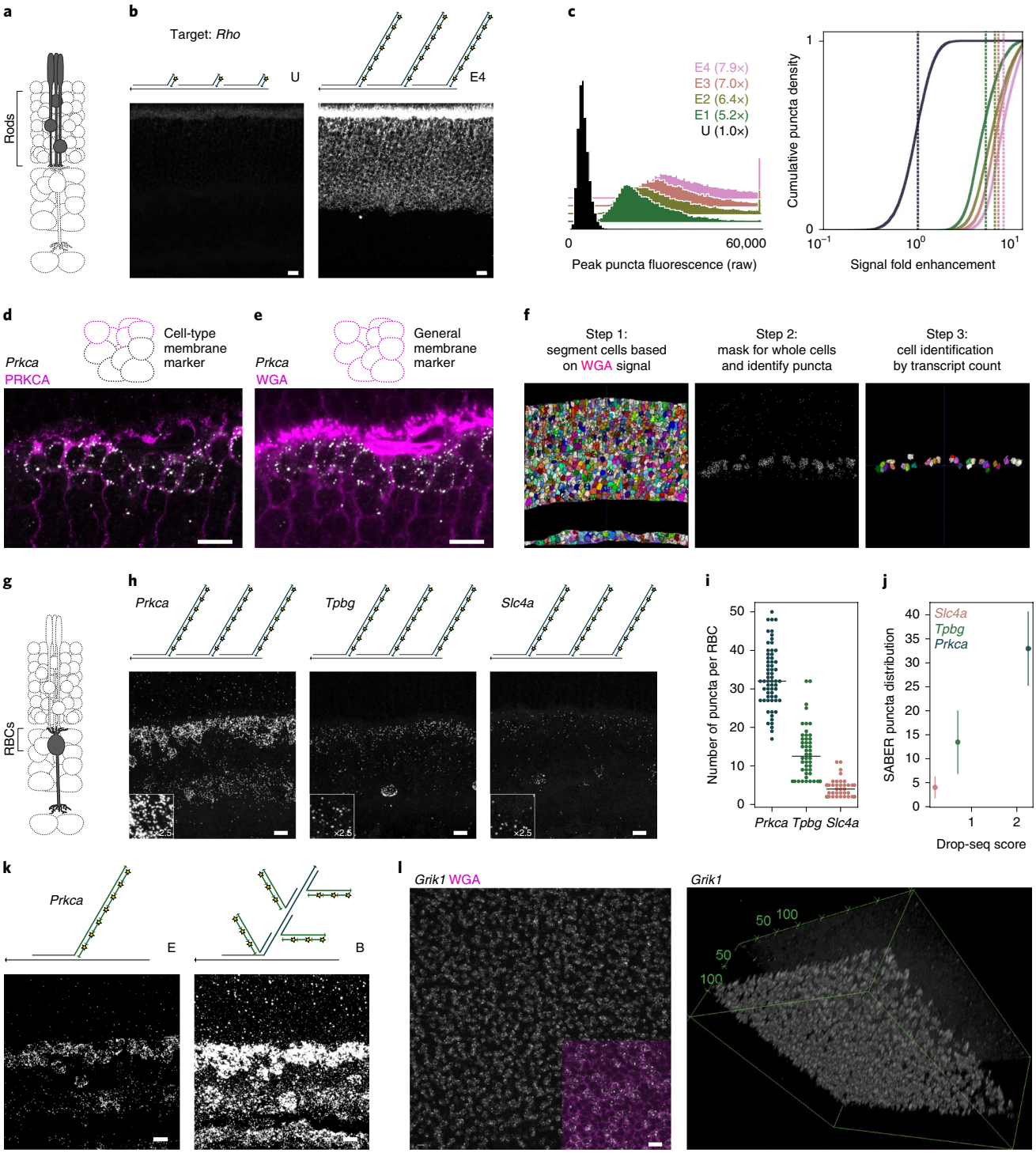

Fig. 3 | Transcript detection and quantification in retina tissue. a, Schematic of the retinal cell type targeted (rods). **b**, SABER-FISH detection of *Rho* transcripts with an unextended probe set versus PER-extended probes (E4). **c**, Quantification of SABER-FISH signal intensity for the detection of *Rho* transcripts with the unextended probe and probes of varying concatemer lengths (E1–E4). Lines corresponding to the mean are shown on the distributions. $n_{(puncta)}$: $n_{(U)}$ = 11,159; $n_{(E1)}$ = 16,426; $n_{(E2)}$ = 19,848; $n_{(E3)}$ = 16,217; $n_{(E4)}$ = 18,051. **d**, Combined detection of *Prkca* transcripts using SABER-FISH and detection of PRKCA protein using immunofluorescence demonstrating the specificity of transcript detection and the localization of transcripts relative to cell boundaries. **e**, Outlining by fluorophore-conjugated WGA of cell bodies in the retina. **f**, Computational pipeline for the detection and assignment of puncta to discrete cells in 3D tissue sections using cell segmentation[41] and a custom MATLAB pipeline (*PD3D*). **g**, Schematic of the retinal cell type targeted (RBCs). **h**, SABER-FISH detection of transcripts for three genes with different expression levels and highly enriched expression in RBCs. **i**, Swarm plot of SABER puncta per RBC with lines indicating median values. **j**, For the three markers, transcript counts per RBC as detected by SABER (*y* axis) are plotted against the average number of transcripts detected per RBC in a Drop-seq dataset ('Drop-seq score'). These results illustrate the similar relative transcript abundance between methods[40]. Means ± s.d. of SABER puncta per cell are shown. $n_{(cells)}$: $n_{(Slc4a)}$ = 45; $n_{(Tpbg)}$ = 48; $n_{(Prkca)}$ = 63. **k**, Detection of *Prkca* transcript with and without branch amplification. **l**, Detection in whole-mount retina of *Grik1* transcript. Left, maximum intensity projection of the en face view in the inner nuclear layer; the inset shows WGA counterstain (magenta). Right, 3D volume rendering of a *z*-stack. Scale bars, 10 µm.

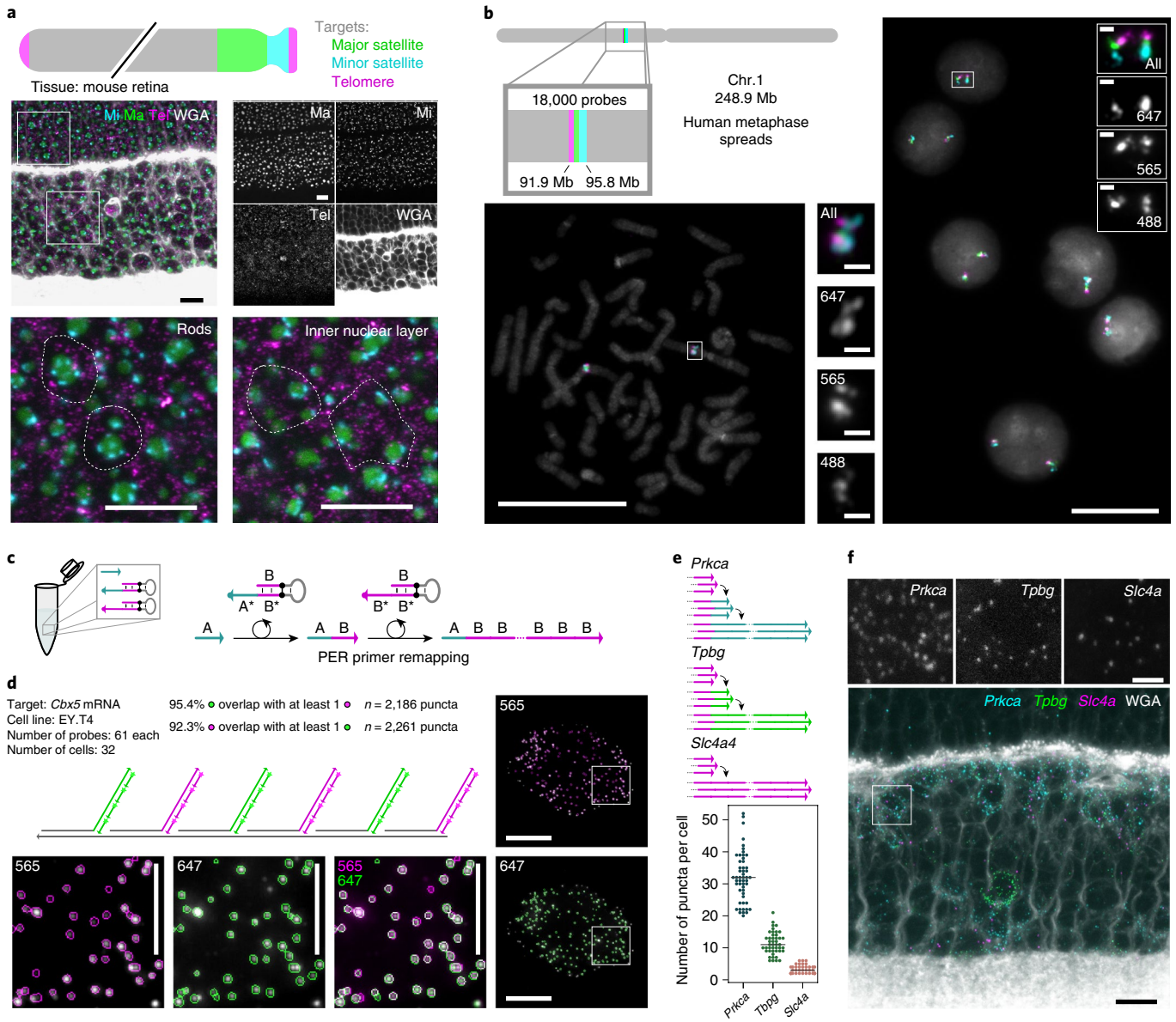

Fig. 4 | SABER enables spectrally multiplexed imaging. a, Multiplexed SABER-FISH in mouse retina. Mouse major satellite, minor satellite and telomere chromosomal regions were detected with orthogonal SABER concatemers. Magnified views show distinct organization of these chromosome regions in rods compared with inner nuclear layer cells. Dashed outlines indicate approximate cell boundaries based on WGA staining. Scale bars, 10 µm. Ma, major satellite; Mi, minor satellite; Tel, telomere. **b**, Multiplexed SABER-FISH on metaphase spreads. Three adjacent positions on human chromosome 1 were visualized using a bridge strategy (Fig. 1d) in metaphase spreads and interphase cells. Scale bars, 20 µm. **c**, Primer remapping with PER. Primers (for example, primers with domain **A**) can be concatemerized with a different repetitive sequence (for example, primers with domain **B**) using a stepwise PER hairpin (the given example appends **B** to **A**)[30] and a standard repetitive hairpin. **d**, Single-molecule colocalization. The three images at bottom left are expanded views of the top and bottom images to the right. Primer remapping was used to map two halves of the *Cbx5* probe pool (used in Fig. 2) to distinct concatemer sequences, and two-color colocalization was visualized (Supplementary Fig. 6b) and quantified. In total, 92.3% of identified puncta in the 565-nm channel ovelapped with puncta in the 647-nm channel, and 95.4% of identified puncta in the 647-nm channel overlapped with puncta in the 565-nm channel. Scale bars, 10 µm (right top and bottom) and 5 µm (expanded views). $n_{(puncta)}$: $n_{(565)} = 2{,}261$ and $n_{(647)} = 2{,}186$. **e**, Primer remapping and three-color visualization in retina tissue. The *Tpbg* and *Prkca* probe sets from Fig. 3 were remapped to two new primers to enable simultaneous visualization and quantification of *Prkca*, *Tpbg* and *Slc4a* transcripts. Lines corresponding to the median are shown on the distributions. $n_{(cells)}$: $n_{(Slc4a)} = 38$; $n_{(Tpbg)} = 45$; $n_{(Prkca)} = 52$. **f**, Representative images of the experiment described in **e**. The top three images are expanded views of the outlined region in the bottom image. Scale bars, 2.5 µm (top) and 10 µm (bottom).

SABER puncta in 3D (Supplementary Fig. 4c) with robust thresholding (Supplementary Fig. 4d). Cells could then be assigned cellular identities on the basis of both transcript counts of marker genes and laminar position in the tissue (Supplementary Fig. 4e). While WGA-based segmentation is limited by the inability to resolve neuronal processes, this limitation also applies to dissociated single retinal cells, and it is therefore a relevant method for use in comparisons with scRNA-seq.

We selected three transcripts for quantification that are highly enriched among RBCs[40] (Fig. 3g) and that are expressed at low (*Slc4a*), moderate (*Tpbg*), or high (*Prkca*) levels (Supplementary Fig. 4b). After imaging (Fig. 3h) and transcript quantification

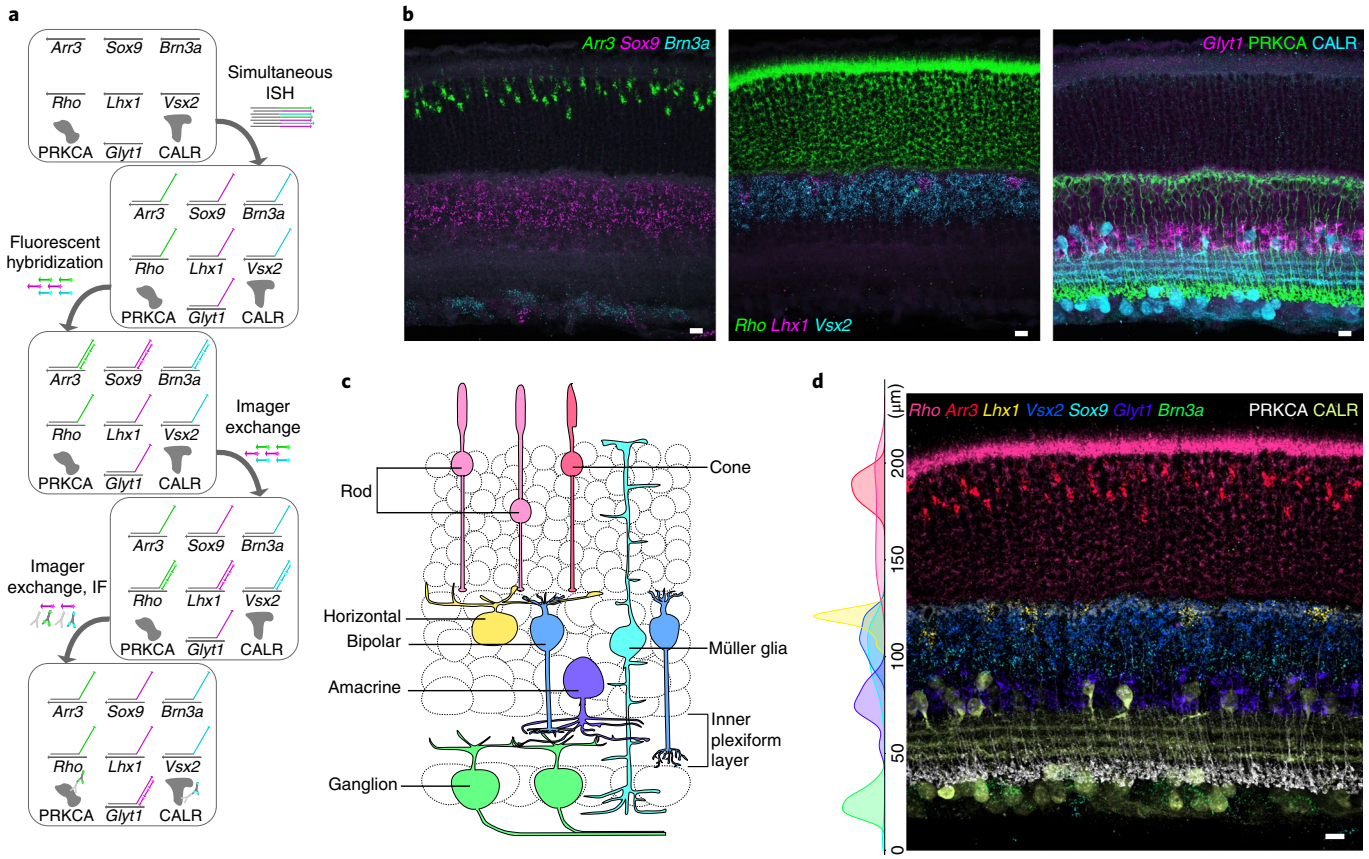

Fig. 5 | Exchange-SABER for detection of cell types in retina tissue. a, Workflow for serial FISH detection of seven transcripts and immunofluorescence (IF) detection of two protein targets. **b**, Three FISH detection cycles for identification of seven retinal cell populations. Immunofluorescence was performed after the third FISH detection. **c**, Schematic of the retinal cell classes detected. **d**, Right, all nine channels overlaid following puncta thresholding, with additional tissue autofluorescence background subtracted by a Gaussian filter masking channels around detected puncta. Left, distributions of marker-positive segmented cells plotted by distance from the inner limiting membrane. $n_{(cells)} = 649$. Scale bars, 10 μm.

(Fig. 3i), we found that the relative transcript abundance for these genes in RBCs as detected by SABER-FISH closely paralleled the relative abundance detected by Drop-seq (Fig. 3j). Sampling of transcripts by SABER was approximately 15-fold higher than was detected in cells profiled using Drop-seq, where cells had been sequenced to an average depth of 8,200 reads per cell for comprehensive classification of bipolar cell types (50-fold-deeper sequencing of Drop-seq libraries improves transcript detection probability by up to approximately twofold[40]). We also observed an 8.8-fold increase in signal intensity using a single round of branching compared with simple extension of the *Prkca* probe set (Fig. 3k and Supplementary Fig. 4f). Transcript counts for *Prkca* detected using branched probes were similar to those detected with the unbranched condition (Supplementary Fig. 4g) and still closely paralleled Drop-seq values (Supplementary Fig. 4h). Branching also permitted robust detection of transcripts with a 12-oligonucleotide probe set (Supplementary Fig. 4i). A concern in the application of pre-extended probes to tissue was the ability of long DNA strands to penetrate tissues. We tested SABER-FISH in formaldehyde-fixed flat-mounted retinas (~150-μm thickness), modifying the tissue-section protocol to have longer incubation and wash times, and observed effective labeling of mRNA in bipolar cells of the inner nuclear layer (Fig. 3l and Supplementary Fig. 5a) for a variety of probe lengths (see Supplementary Fig. 5b for quantification and Supplementary Fig. 5c for images).

SABER enables spectrally multiplexed imaging. Probes deployed against distinct targets can be visualized simultaneously by appended orthogonal concatemer sequences that are detectable by imager oligonucleotides with distinct fluorophores. Three repetitive regions of mouse chromosomes—major satellite, minor satellite and telomere—were visualized simultaneously in mouse retinal tissue using this approach (Fig. 4a), permitting observation of the distinctive chromatin architecture of rod photoreceptors[42]. Another three-color visualization was performed in human metaphase spreads and interphase cells to target three adjacent positions on chromosome 1 (Fig. 4b). In total, 18,000 probes targeting a 3.9-Mb region were mapped to three colors, which all colocalized as expected. Intronic and exonic sequences were also separately detected for *Dll1* mRNA transcripts in developing retina (Supplementary Fig. 6a), a distinction that is useful as a method to probe transcription kinetics.

We previously showed how PER cascades can be programmed to autonomously undergo differential synthesis pathways by changing the hairpins present in solution[30]. The flexibility to program sequences allows us to take existing probe sets and change the sequence of the PER concatemer synthesized onto them. Figure 4c shows an example of how a primer **A** can be mixed with two hairpins to produce a concatemer with repeats of sequence **B**. The first of two hairpins appends the **B** sequence 3′ from the **A** sequence, and then a second hairpin repeatedly adds the **B** sequence to generate a concatemer with a different PER primer sequence than the original one. See the Supplementary Protocols for further information about designing these PER primer remapping reactions.

This remapping strategy is useful for cases where multiple probe sets have been synthesized with the same PER primer on the 3′ ends of the oligonucleotides but must be independently detected.

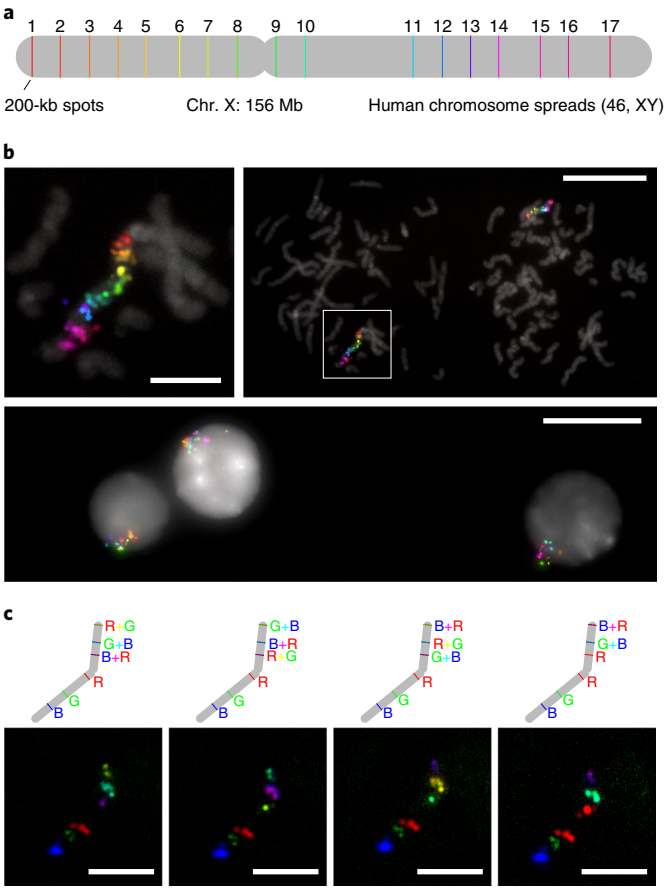

Fig. 6 | Sequential imaging of chromosomal targets using Exchange-SABER. a, Schematic of 17 targeted regions along the human X chromosome (width to scale). Each set of probes per spot had different 42-nucleotide oligomer barcode sequences appended to their 3′ ends (Fig. 1d). Seventeen 42-nucleotide oligomer bridge sequences concatemerized with 17 different PER primers were simultaneously hybridized. **b**, Seventeen-color overlays on 4′,6-diamidino-2-phenylindole (DAPI). A representative metaphase spread is shown overlaid on DAPI at two length scales (top left and top right). Interphase cells showing the X chromosome territories were also captured (bottom). **c**, Combinatorial six-color SABER imaging. As a step toward further increasing multiplexing with SABER amplification, we demonstrated mapping for six of the spots on the chromosome to four different six-color combinations. Scale bars, 5 µm (spreads) or 20 µm (fields of view).

With the use of PER primer remapping to impart new, orthogonal concatemer sequences on some of these probe sets, each can be detected as a distinct color despite having an identical 9-nucleotide sequence at the 5′ end of the concatemer. The *Cbx5* probe set (used in Fig. 2) was split into two pools, and each pool was remapped to a new primer sequence. This enabled a two-color visualization of *Cbx5* transcripts (Fig. 4d and Supplementary Fig. 6b), where half of the probes were mapped to the 565-nm channel and the other half were mapped to the 647-nm channel. We found that 92.3% of puncta identified in the 565-nm channel overlapped with puncta in the 647-nm channel, and conversely that 95.4% of puncta identified in the 647-nm channel overlapped with puncta in the 565-nm channel. These numbers further indicate that SABER-FISH probes can enable the detection of a large fraction of available transcripts at the single-molecule level. We also evaluated primer remapping for two of the three RBC-expressed genes evaluated in Fig. 3 (*Prkca* and *Tpbg*) to simultaneously detect the three transcript species for probe extensions that were originally synthesized with identical primers (see Fig. 4e and Supplementary Fig. 6c for analysis and Fig. 4f for images).

Exchange-SABER enables fast exchange for highly multiplexed sequential imaging in cells and tissues. Higher levels of multiplexing can be achieved by iterative detection of nucleic acid targets using DNA-Exchange[8–10]. We use formamide to rapidly destabilize short fluorescent imager strands without destabilizing the primary probe, thus permitting reuse of spectral channels. By modeling the melting temperatures of 20-nucleotide oligomer imagers, 42-nucleotide oligomer bridge sequences and FISH probe sequences (Supplementary Fig. 7a), we predicted that 50–60% formamide in 1× PBS would effectively destabilize imagers without significantly affecting the underlying stability of the probe or 42-nucleotide oligomer bridge sequence.

We tested this approach, which we call Exchange-SABER, in retinal tissue. Neural tissues typically display high cell-type heterogeneity, requiring multiplexed detection methods for comprehensive identification of cellular populations. We aimed to detect all seven major cell classes in the retina (cone, rod, horizontal, bipolar, amacrine, ganglion and Müller glia cells) using SABER probes against established markers. A pool of seven primary FISH probe sets was hybridized simultaneously and detected in three sequential rounds of secondary hybridization of fluorescent oligonucleotides (Fig. 5a). Exchange of imager oligonucleotides occurred effectively in tissues, permitting reuse of spectral channels (Fig. 5b), and we observed the expected laminar separation of the cell classes (Fig. 5c) after overlaying and quantifying the channels (Fig. 5d). Following serial detection of FISH probes, protein epitopes were still detectable by immunofluorescence, and tissue integrity appeared well preserved, with sublaminae of the inner plexiform layer (IPL) clearly discernible.

We additionally confirmed that DNase I and Exonuclease I enzymes could be used to strip both primary SABER probes and imagers in tissue, while preserving mRNA integrity, as assayed by the ability to perform a second round of mRNA detection (Supplementary Fig. 7b). Therefore, multiplexing using SABER is achievable either by a large selection of concatemer sequences (Exchange-SABER) or by the ability to recycle concatemer sequences through digestion of primary probes and rehybridization[43]. While the probe-digestion approach is slower than Exchange-SABER, as it requires iterative (long) ISH steps rather than sequential (fast) fluorescent hybridization steps, it allows reuse of the same PER hairpin and imager sequences and is therefore a simple way to reduce the up-front cost of reagents.

We further used Exchange-SABER to directly compare two-color primary concatemer detection with two-color branching-based detection of a non-endogenous target mRNA (*Cas9*; Supplementary Fig. 8a,b) and compared it with the signal from coexpressed green fluorescent protein (GFP; Supplementary Fig. 8c,d) to further confirm the specificity of SABER signals. As expected, all four SABER signals showed strong colocalization (Supplementary Fig. 8e,f), further increasing our confidence that branched and standard SABER-FISH signals correspond to true target transcripts.

We also evaluated Exchange-SABER in human metaphase spreads and interphase cells, with 17 colors targeting seventeen 200-kb regions spread along the human X chromosome (Fig. 6a). Metaphase spreads validate the directional coloring of targets, and interphase cells depict X chromosome territories within their nuclei. In total, 17 colors (six hybridizations) were imaged in 7 h, which included the time taken for stripping, rehybridization, finding fields of view and *z*-stack imaging (Fig. 6b and Supplementary Fig. 9a,b). Such brief incubation times are aided by the improved reaction kinetics conferred by the presence of many imager-binding sites within concatemers, as not all binding sites must be saturated to discern signal.

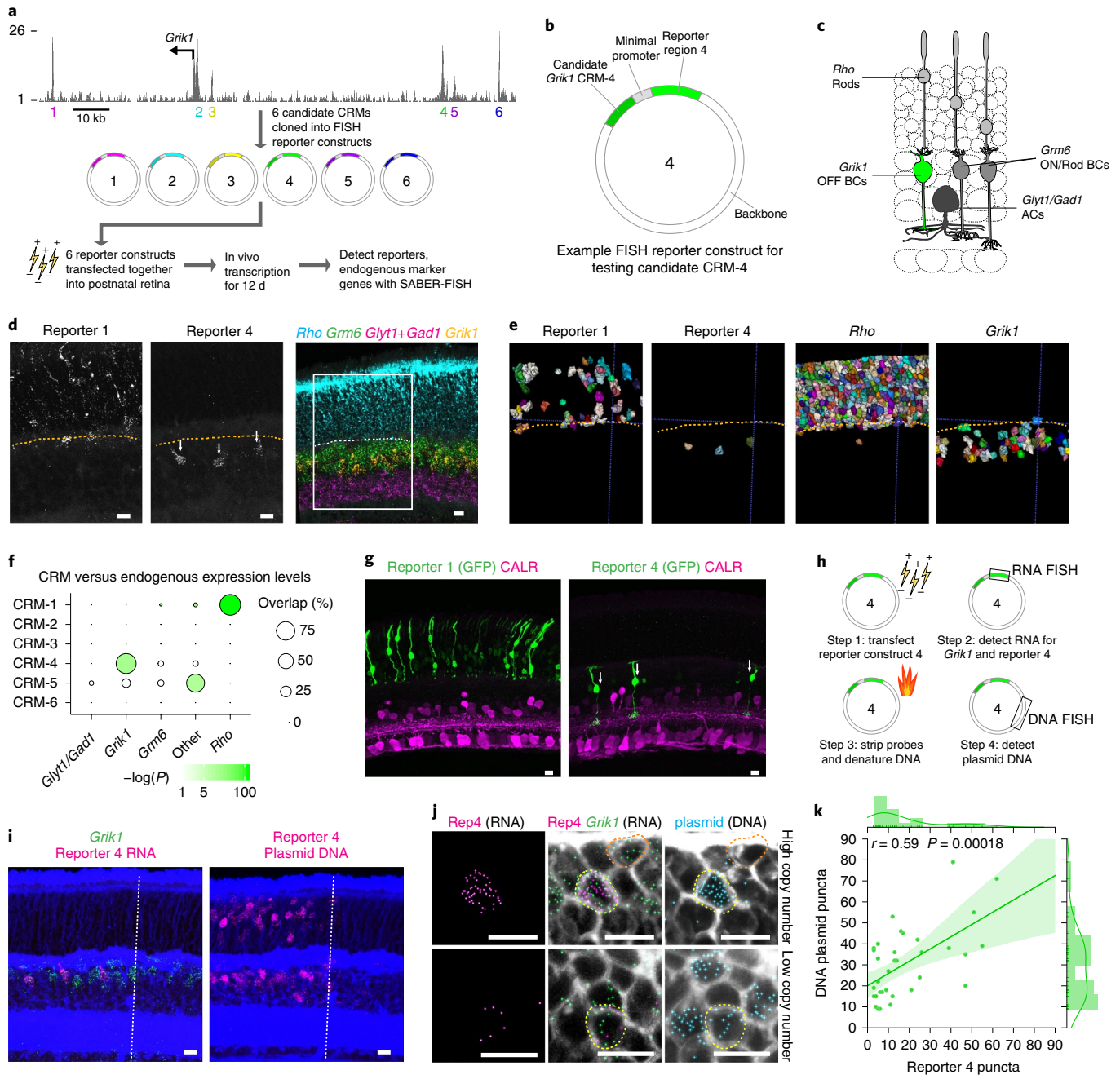

Fig. 7 | SABER-FISH enables detection of in vivo RNA reporters for analysis of enhancer activity. a, Mouse retina DNase I-hypersensitive regions (ENCODE[45]) in the vicinity of the *Grik1* transcription start site and the workflow for the reporter screen experiment. The vertical axis represents absolute read density. **b**, Representation of key components of the reporter plasmid. **c**, Schematic of the neuronal cell types electroporated in the postnatal retina. *Grik1* expression distinguishes OFF bipolar cells from ON bipolar cells (*Grm6*$^+$). **d**, Representative images of two expressed reporters (single channel) and four endogenously expressed genes. The dashed line indicates the approximate position of the outer plexiform layer. The box indicates the area of magnification shown for the images of expression of the single-channel reporter. **e**, Cells expressing relevant reporter and endogenous genes shown after cell segmentation. **f**, Quantification of the percentage of reporter-positive cells that were positive for each marker probed. 'Other' refers to expression in cells not positive for any marker tested and may include Müller glia and type 1 bipolar cells. Dot size corresponds to the percentage of CRM-positive cells that are positive for each endogenous marker. Dot color reflects the *P* value for a hypergeometric test plotted on a logarithmic color scale. $n_{(cells)}$: $n_{(CRM\text{-}1)} = 440$; $n_{(CRM\text{-}4)} = 18$; $n_{(CRM\text{-}5)} = 25$. **g**, Expression of GFP driven by CRM-1 and CRM-4 after retina electroporation. Rods (left) are identifiable by their position in the outer nuclear layer, and OFF bipolar cells (right; arrows) are identifiable by their bipolar morphology and lamination in the upper layers of the IPL, which is labeled by calretinin (CALR). **h**, Experimental design for sequential detection of reporter RNA and DNA. **i**, Representative image of an electroporated retina with detection of reporter 4 RNA, *Grik1* mRNA, and plasmid DNA. The dashed line indicates the approximate location of the electroporation patch boundary. **j**, Magnified images showing detected reporter 4 RNA puncta in cells with *Grik1* expression and plasmid DNA (yellow outline) but not in *Grik1*$^+$ cells lacking plasmid DNA (orange outline). **k**, Quantification of detected reporter 4 RNA puncta plotted against detected plasmid DNA puncta in *Grik1*$^+$ cells. The Pearson correlation coefficient and *P* value are shown. The shaded region indicates the 95% confidence interval. $n_{(cells)} = 35$. Scale bars, 10 μm.

We next took the same metaphase sample and applied new, combinatorial fluorescent hybridizations. Each hybridization targeted the same set of six regions, mapping each of them to one of the three different colors or to the pairwise combinations of the three colors, which we obtained by simultaneously hybridizing complementary imager oligonucleotides conjugated with different fluorophores. This process was repeated four times (~4 h in total), each time with a different six-color mapping (Fig. 6d). The success of this detection scheme indicates that SABER should be compatible with combinatorial imaging strategies for the detection of highly multiplexed and amplified targets.

Application of SABER in a quantitative in situ reporter assay. We next investigated whether the ability of SABER to provide multiplexed, amplified detection of both RNA and DNA sequences in tissues could be applied to reporter assays involving the introduction of exogenous DNA elements. An ideal reporter assay would permit simultaneous quantification of the expression of reporter molecules, the number of introduced DNA constructs encoding the reporters and the expression of endogenous markers. We applied SABER to detect reporter RNAs transcribed from plasmids bearing isolated *cis*-regulatory modules (CRMs). First, reporter sequences were cloned downstream of a minimal promoter and validated independently for the ability to report CRM activity, using upstream insertion of a validated bipolar cell enhancer[44] (Supplementary Fig. 10a). Plasmids were then introduced to the retina by electroporation (Supplementary Fig. 10b).

We applied this reporter set to evaluate the behaviors of previously uncharacterized CRMs using a 10-plex SABER-FISH experiment. We selected for investigation candidate CRMs in the vicinity of the gene *Grik1*, which encodes a kainite-family glutamate receptor subunit with strong and enriched expression in most OFF bipolar cells (types 2, 3a, 3b and 4)[40], as few genetic tools exist to specifically label this population in vivo. Candidate CRMs were identified by inspection of the accessibility of retina chromatin to DNase I (data from the ENCODE project[45]) in a genomic interval proximal to the transcription start site (Fig. 7a). Six candidate DNA sequences (CRM-1 to CRM-6) were inserted independently upstream of distinct reporters, and the reporter set was introduced as a pool into the retina (Fig. 7a,b). We used SABER to detect all six reporters as well as four markers of cell types accessible by electroporation of postnatal retinas (*Grm6*, ON bipolar cells; *Glyt1* and *Gad1*, amacrine cells; *Rho*, rods)[46] (Fig. 7c). Images (Fig. 7d and Supplementary Fig. 10c) and segmentation results (Fig. 7e) indicated that one reporter, corresponding to CRM-4, was selectively expressed in *Grik1*$^+$ cells (Supplementary Fig. 10d). A second reporter (CRM-1) instead showed abundant and specific expression in *Rho*$^+$ cells (rods) (Fig. 7d,e). We estimated the specificity of CRM activity in different cell types by comparing reporter expression with the expression of endogenous cell-type markers. We first calculated the abundances of each cell type, determining that 9% of electroporated cells expressed endogenous *Grik1* transcripts. A hypergeometric test was used to evaluate the probability of observing the empirically determined positive patterns for each CRM, yielding highly significant *P* values ($P = 1.27 \times 10^{-125}$ for CRM-1/*Rho* and $P = 1.03 \times 10^{-15}$ for CRM-4/*Grik1*; Fig. 7f). The specificity of CRM activity was also confirmed by a GFP fluorescence assay (Fig. 7g).

We investigated whether SABER could be used to simultaneously detect reporter-encoding plasmids and reporter transcripts. Commonly used methods for dense introduction of exogenous DNAs in vivo (for example, electroporation, adeno-associated viruses and cationic lipids) can result in a broad distribution of DNA copy number per cell, with cell-type-specific biases in transfection rates. This variability can impede assessment of CRM activity (reporter transcripts divided by reporter DNA). Measurements of enhancer specificity must account for the abundances of different cell types among the transfected cells, which may also be highly variable. We applied simultaneous detection of the reporter RNA and the plasmid DNA backbone to determine distributions of transfected cell types and plasmid load (Fig. 7h). The CRM-4 reporter was singly electroporated into the retina, followed by detection and quantification of reporter RNA, *Grik1* transcript and a 2.8-kb region of the plasmid backbone in the same electroporated cell populations (Fig. 7i). We examined the relationship between the number of plasmids and the number of reporter transcripts in *Grik1*$^+$ cells (Fig. 7j) and observed a significant correlation (Pearson correlation coefficient of 0.59, $P = 0.00018$; Fig. 7k) that was not observed in comparisons of plasmid copy number with endogenous *Grik1* expression (Supplementary Fig. 10e,f). Variation in transcript number per plasmid may represent selective silencing of plasmids in particular cells or differences in CRM-4 activity between distinct *Grik1*-expressing OFF bipolar cell types.

Discussion

The PER method is a versatile tool for creating user-defined assembly of short sequences using a catalytic hairpin structure. Here we apply the telomerase-like mode of PER to achieve enhanced FISH signals. PER is used to synthesize concatemers of user-defined length on single-molecule FISH and Oligopaint-style tiling probes in vitro. These concatemers provide a scaffold for concentrating fluorescent signal via secondary hybridization, a method we name SABER. Through the application of SABER to a large array of different sample and target types, we demonstrated the strengths and flexibility of this approach: (1) programmable levels of signal amplification between 5- and 450-fold; (2) multiplexing with at least 17 orthogonal concatemers applied simultaneously; (3) high detection efficiency in tissue; and (4) applicability to diverse targets (RNA and DNA, endogenous and exogenously introduced). Additionally, SABER can also be applied for detecting protein targets via DNA-conjugated antibodies, as described in an upcoming work[47].

SABER was also practical to apply in terms of workflow and cost. SABER works with minimally pre-treated tissues using standard hybridization protocols, and we effectively labeled thick tissue sections and whole retinas without the application of tissue clearing or gels. Probe sets ordered unpurified and unmodified can be amplified in bulk using PER in vitro with a single enzymatic step, allowing enough material for dozens of experiments to be prepared in one step, avoiding the need for long amplification steps in situ and reducing cost. The combined cost of all oligonucleotides and enzymes is currently estimated to be less than $5 per target per experiment (120 µl ISH solution) and could be further reduced with additional optimization and bulk synthesis (Supplementary Note).

The analytic pipeline demonstrated here is similarly straightforward to use. 3D cell segmentation combined with SABER permitted quantification of transcripts on a single-cell level, and relative transcript abundance closely correlated with Drop-seq measurements. SABER is therefore well suited to accompany scRNA-seq in transcriptomic studies. SABER, which is compatible with immunofluorescence, can be used to link populations defined using scRNA-seq to positions in tissues such that morphological stains or labels that permit post hoc identification of recorded cells can be integrated with cell-type identification.

Detection of complex pools of reporters or barcodes is another area where effective multiplexed FISH technologies can be applied. In cell culture, FISH-based barcode detection has been used for lineage analysis[48], and barcode reading is an element of STARmap probe design[29]. Here we demonstrated the utility of SABER for assaying the activity of isolated candidate enhancer sequences. Simultaneous detection of reporter expression and cell-type markers with single-cell resolution was required for assessing the cell-type specificity of CRM activity. Using SABER, we were able to detect reporters across a broad range of expression levels and assay

the copy number of DNA plasmids in the same cells, thus providing a tool to quantify enhancer strength and specificity. As an effective and simple method to robustly detect RNA and DNA sequences in cells and tissue, SABER enables characterization of the abundance, identities and localization of complex sets of endogenous and introduced nucleic acids.

In cases where targets are spatially separated, there is further opportunity to combine SABER amplification with multiple-round combinatorial barcoding. Such barcoding methods allow an exponential number of unique, non-overlapping targets to be visualized in a linear number of rounds[14–17]. These multiplexing strategies could benefit from signal amplification, and recent studies have been able to combine signal amplification with combinatorial barcoding (for example, sequential FISH combined with HCR[43] and RCA paired with a sequencing-by-ligation readout[29]). For hybridization-based, high-targeting-efficiency spatial genomic and transcriptomic methods, SABER may offer the unique potential for rapid one-step deployment of a large set of orthogonal amplifiers for subsequent combinatorial readout.

Online content

Any methods, additional references, Nature Research reporting summaries, source data, statements of code and data availability and associated accession codes are available at https://doi.org/10.1038/s41592-019-0404-0.

Received: 27 October 2018; Accepted: 3 April 2019;
Published online: 20 May 2019

References

1. Pardue, M. L. & Gall, J. G. Molecular hybridization of radioactive DNA to the DNA of cytological preparations. *Proc. Natl Acad. Sci. USA* **64**, 600–604 (1969).
2. Riegel, M. Human molecular cytogenetics: from cells to nucleotides. *Genet. Mol. Biol.* **37**, 194–209 (2014).
3. Bolzer, A. et al. Three-dimensional maps of all chromosomes in human male fibroblast nuclei and prometaphase rosettes. *PLoS Biol.* **3**, 0826–0842 (2005).
4. Femino, A. M., Fay, F. S., Fogarty, K. & Singer, R. H. Visualization of single RNA transcripts in situ. *Science* **280**, 585–590 (1998).
5. Raj, A., van den Bogaard, P., Rifkin, S. A., van Oudenaarden, A. & Tyagi, S. Imaging individual mRNA molecules using multiple singly labeled probes. *Nat. Methods* **5**, 877–879 (2008).
6. Schröck, E. et al. Multicolor spectral karyotyping of human chromosomes. *Science* **273**, 494–497 (1996).
7. Lubeck, E. & Cai, L. Single-cell systems biology by super-resolution imaging and combinatorial labeling. *Nat. Methods* **9**, 743–748 (2012).
8. Jungmann, R. et al. Multiplexed 3D cellular super-resolution imaging with DNA-PAINT and Exchange-PAINT. *Nat. Methods* **11**, 313–318 (2014).
9. Schueder, F. et al. Universal super-resolution multiplexing by DNA exchange. *Angew. Chem. Int. Ed. Engl.* **56**, 4052–4055 (2017).
10. Wang, Y. et al. Rapid sequential in situ multiplexing with DNA exchange imaging in neuronal cells and tissues. *Nano Lett.* **17**, 6131–6139 (2017).
11. Wang, S. et al. Spatial organization of chromatin domains and compartments in single chromosomes. *Science* **353**, 598–602 (2016).
12. Bintu, B. et al. Super-resolution chromatin tracing reveals domains and cooperative interactions in single cells. *Science* **362**, eaau1783 (2018).
13. Codeluppi, S. et al. Spatial organization of the somatosensory cortex revealed by osmFISH. *Nat. Methods* **15**, 932–935 (2018).
14. Lubeck, E., Coskun, A. F., Zhiyentayev, T., Ahmad, M. & Cai, L. Single-cell in situ RNA profiling by sequential hybridization. *Nat. Methods* **11**, 360–361 (2014).
15. Chen, K. H., Boettiger, A. N., Moffitt, J. R., Wang, S. & Zhuang, X. Spatially resolved, highly multiplexed RNA profiling in single cells. *Science* **348**, aaa6090 (2015).
16. Levesque, M. J. & Raj, A. Single-chromosome transcriptional profiling reveals chromosomal gene expression regulation. *Nat. Methods* **10**, 246–248 (2013).
17. Shah, S. et al. Dynamics and spatial genomics of the nascent transcriptome by intron seqFISH. *Cell* **174**, 363–376 (2018).
18. Kerstens, H. M., Poddighe, P. J. & Hanselaar, A. G. A novel in situ hybridization signal amplification method based on the deposition of biotinylated tyramine. *J. Histochem. Cytochem.* **43**, 347–352 (1995).
19. Player, A. N., Shen, S. P., Kenny, D., Antao, V. P. & Kolberg, J. A. Single-copy gene detection using branched DNA (bDNA) in situ hybridization. *J. Histochem. Cytochem.* **49**, 603–611 (2001).
20. Wang, F. et al. RNAscope: a novel in situ RNA analysis platform for formalin-fixed, paraffin-embedded tissues. *J. Mol. Diagn.* **14**, 22–29 (2012).
21. Beliveau, B. J. et al. Single-molecule super-resolution imaging of chromosomes and in situ haplotype visualization using Oligopaint FISH probes. *Nat. Commun.* **6**, 7147 (2015).
22. Lizardi, P. et al. Mutation detection and single-molecule counting using isothermal rolling-circle amplification. *Nat. Genet.* **19**, 225–232 (1998).
23. Dirks, R. M. & Pierce, N. A. Triggered amplification by hybridization chain reaction. *Proc. Natl Acad. Sci. USA* **101**, 15275–15278 (2004).
24. Choi, H. M. T. et al. Programmable in situ amplification for multiplexed imaging of mRNA expression. *Nat. Biotechnol.* **28**, 1208–1212 (2010).
25. Choi, H. M., Beck, V. A. & Pierce, N. A. Next-generation in situ hybridization chain reaction: higher gain, lower cost, greater durability. *ACS Nano* **8**, 4284–4294 (2014).
26. Shah, S. et al. Single-molecule RNA detection at depth via hybridization chain reaction and tissue hydrogel embedding and clearing. *Development* **92**, 2862–2867 (2016).
27. Rouhanifard, S. H. et al. ClampFISH detects individual nucleic acid molecules using click chemistry–based amplification. *Nat. Biotechnol.* **37**, 84–89 (2018).
28. Nagendran, M., Riordan, D. P., Harbury, P. B. & Desai, T. J. Automated cell-type classification in intact tissues by single-cell molecular profiling. *eLife* **7**, e30510 (2018).
29. Wang, X. et al. Three-dimensional intact-tissue sequencing of single-cell transcriptional states. *Science* **361**, eaat5691 (2018).
30. Kishi, J. Y., Schaus, T. E., Gopalkrishnan, N., Xuan, F. & Yin, P. Programmable autonomous synthesis of single-stranded DNA. *Nat. Chem.* **10**, 155–164 (2018).
31. Beliveau, B. J. et al. Versatile design and synthesis platform for visualizing genomes with Oligopaint FISH probes. *Proc. Natl Acad. Sci. USA* **109**, 21301–21306 (2012).
32. Lee, C. S., Davis, R. W. & Davidson, N. A physical study by electron microscopy of the terminally repetitious, circularly permuted DNA from the coliphage particles of *Escherichia coli* 15. *J. Mol. Biol.* **48**, 1–22 (1970).
33. Beliveau, J. et al. OligoMiner provides a rapid, flexible environment for the design of genome-scale oligonucleotide in situ hybridization probes. *Proc. Natl Acad. Sci. USA* **115**, E2183–E2192 (2018).
34. Xu, Q., Schlabach, M. R., Hannon, G. J. & Elledge, S. J. Design of 240,000 orthogonal 25mer DNA barcode probes. *Proc. Natl Acad. Sci. USA* **106**, 2289–2294 (2009).
35. Dirks, R. M. & Pierce, N. A. A partition function algorithm for nucleic acid secondary structure including pseudoknots. *J. Comput. Chem.* **24**, 1664–1677 (2003).
36. Dirks, R. M. & Pierce, N. A. An algorithm for computing nucleic acid base-pairing probabilities including pseudoknots. *J. Comput. Chem.* **25**, 1295–1304 (2004).
37. Dirks, R. M., Bois, J. S., Schaeffer, J. M., Winfree, E. & Pierce, N. A. Thermodynamic analysis of interacting nucleic acid strands. *SIAM Rev.* **49**, 65–88 (2007).
38. Carpenter, A. E. et al. CellProfiler: image analysis software for identifying and quantifying cell phenotypes. *Genome Biol.* **7**, R100 (2006).
39. Macosko, E. Z. et al. Highly parallel genome-wide expression profiling of individual cells using nanoliter droplets. *Cell* **161**, 1202–1214 (2015).
40. Shekhar, K. et al. Comprehensive classification of retinal bipolar neurons by single-cell transcriptomics. *Cell* **166**, 1308–1323 (2016).
41. Mosaliganti, K. R., Noche, R. R., Xiong, F., Swinburne, I. A. & Megason, S. G. ACME: automated cell morphology extractor for comprehensive reconstruction of cell membranes. *PLoS Comput. Biol.* **8**, e1002780 (2012).
42. Solovei, I. et al. Nuclear architecture of rod photoreceptor cells adapts to vision in mammalian evolution. *Cell* **137**, 356–368 (2009).
43. Shah, S., Lubeck, E., Zhou, W. & Cai, L. In situ transcription profiling of single cells reveals spatial organization of cells in the mouse hippocampus. *Neuron* **92**, 342–357 (2016).
44. Emerson, M. M. & Cepko, C. L. Identification of a retina-specific Otx2 enhancer element active in immature developing photoreceptors. *Dev. Biol.* **360**, 241–255 (2011).
45. ENCODE Project Consortium. An integrated encyclopedia of DNA elements in the human genome. *Nature* **489**, 57–74 (2012).
46. Matsuda, T. & Cepko, C. L. Electroporation and RNA interference in the rodent retina in vivo and in vitro. *Proc. Natl Acad. Sci. USA* **101**, 16–22 (2004).
47. Saka, S. K. et al. Highly multiplexed in situ protein imaging with signal amplification by Immuno-SABER. *Nat. Biotechnol.* (in the press).
48. Frieda, K. L. et al. Synthetic recording and in situ readout of lineage information in single cells. *Nature* **541**, 107–111 (2017).

Acknowledgements

The authors thank B. Fields, S. Kennedy, J.A. Abed, T. Wu, T. Ferrante, N. Liu, F. Dannenberg, M. Cicconet, P.M. Llopis and the Microscopy Resources on the North Quad (MicRoN) at Harvard Medical School for discussions and technical support.

We also thank the ENCODE consortium and J. Stamatoyannopoulos (University of Washington) for retina DHS data. This work was supported by the National Institutes of Health (under grants 1R01EB018659-01 to P.Y., 1UG3HL145600 to P.Y., 1R01GM124401 to P.Y., 1U01MH106011-01 to P.Y., 1DP1GM133052 to P.Y., 5K99EY028215-02 to S.W.L. and a T32 training grant GM096911 supporting E.R.W.), the Office of Naval Research (under grants N00014-16-1-2410 to P.Y. and N00014-18-1-2549 to P.Y.), the National Science Foundation (under grant CCF-1317291 to P.Y. and a Graduate Research Fellowship to J.Y.K.), the Howard Hughes Medical Institute (C.L.C.), the Damon Runyon Cancer Research Foundation (under a fellowship to B.J.B.), the Uehara Memorial Foundation (under a fellowship to H.M.S.), the Human Frontier Science Program (under fellowship LT000048/2016-L to S.K.S.), EMBO (under fellowship ALTF 1278-2015 to S.K.S.) and the Wyss Institute's Molecular Robotics Initiative (MRI) (P.Y., J.Y.K. and B.J.B.).

Author contributions

J.Y.K., S.W.L., B.J.B., E.R.W., C.L.C. and P.Y. conceived the study. J.Y.K. and B.J.B. designed SABER probes, designed and executed cell experiments and analyzed cell data. S.W.L. designed and executed tissue experiments. E.R.W. developed the analytical pipeline and methods for tissue cell segmentation and puncta quantification. J.Y.K., S.W.L., B.J.B., E.R.W., A.Z., S.K.S., H.M.S. and Y.W. contributed to optimizing and performing experimental protocols and obtaining data. J.Y.K., S.W.L., B.J.B., E.R.W., C.L.C. and P.Y. wrote the manuscript. All authors edited and approved the manuscript. C.L.C. and P.Y. supervised the work.

Competing interests

A provisional US patent has been filed based on this work (PCT/US2018/013019). P.Y. is cofounder of Ultivue, Inc. and NuProbe Global.

Additional information

Supplementary information is available for this paper at https://doi.org/10.1038/s41592-019-0404-0.

Reprints and permissions information is available at www.nature.com/reprints.

Correspondence and requests for materials should be addressed to B.J.B., C.L.C. or P.Y.

Publisher's note: Springer Nature remains neutral with regard to jurisdictional claims in published maps and institutional affiliations.

Methods

All procedures were performed at room temperature, except where otherwise specified. Step-by-step protocols for probe design, oligonucleotide ordering, PER concatemerization, RNA FISH in cells, and RNA FISH in tissues can be found in the Supplementary Protocols.

Cell culture. MRC-5 (human; ATCC, CCL-171) and HEK293T (human; ATCC, CRL-1573) cells were grown in DMEM (Gibco, cat. no. 10564) supplemented with 10% (vol/vol) serum (Gibco, cat. no. 10437 for MRC-5 and Peak Serum PS-FB2 for HEK293T), 50 U ml^{-1} penicillin, and 50 µg ml^{-1} streptomycin (Gibco, cat. no. 15070). EY.T4 embryonic fibroblasts (mouse)[49] were grown in DMEM supplemented with 15% (vol/vol) serum, 50 U ml^{-1} penicillin and 50 µg ml^{-1} streptomycin. All cells were cultured at 37 °C in the presence of 5% CO_2.

Tissue. All animal experiments were conducted in compliance with protocol IS00001679, approved by the Institutional Animal Care and Use Committees at Harvard University. Experiments were performed on tissue collected from wild-type male and female CD1 IGS mice (Charles River). Tissues were collected at postnatal day (P) 17 for all experiments with the exception of electroporated retinas used for reporter assays (P13) and retinas in Supplementary Fig. 5 (P25).

DNA and RNA FISH probe design. Oligopaint FISH probe sets[31] targeting mouse mRNAs, human chromosome 1 and the human X chromosome were discovered using the OligoMiner pipeline[33] run with the 'balance' settings and accessed from the mm10 and hg38 whole-genome probe sets hosted at https://yin.hms.harvard.edu/oligoMiner/list.html. For RNA FISH probes, the genomic locations of the exons and/or introns of the target gene were acquired from the UCSC Genome Browser[50] and used in combination with the 'intersectBed' utility of BedTools[51] to isolate probe oligonucleotides targeting the RNA features of interest. As the aforementioned database of probe sequences exclusively contain positive-strand information, in cases where the desired RNA target also carried positive-strand sequence, the OligoMiner script 'probeRC' was used to convert the probe sequences to their reverse complements. Oligopaint probes targeting the six non-endogenous reporter RNA sequences and the reporter plasmid DNA backbone were also designed using OligoMiner, with the 'blockParse' script run with 'balance' settings (-t 42 -T 47 -l 36 -L 41), aligned to the mm10 reference genome using Bowtie2 (ref. [52]) with '--very-sensitive-local' settings processed by 'outputClean' using 'zero mode / −0' and finally compared against a dictionary of all 18-nucleotide oligomers occurring in mm10 produced by Jellyfish 2.0 (ref. [53]), with candidate probes containing an 18-nucleotide oligomer occurring more than two times in mm10 filtered out. Oligonucleotide probes targeting the mouse major satellite, minor satellite and telomere repeats were adapted from ref. [54]. Step-by-step instructions for probe set design can be found in the Supplementary Protocols.

Design of 42-nucleotide oligomer bridge sequences. The 42-nucleotide oligomer bridge sequences were drawn from blocks of orthogonal barcode sequences[34] catenated together. They were then checked against target genomes using the same vetting process (Bowtie[52] and Jellyfish[53]) used for candidate probe sequences (see above), as well as with BLAST[55]. NUPACK[35–37] ('prob' and 'complexes' executables) was used to evaluate and subsequently screen the single-strandedness of probes and duplexing probabilities, respectively. See Supplementary Table 1 for a complete list of the designed 42-nucleotide oligomer bridge sequences.

PER primer sequence design. A set of three-letter primer sequences were designed to have a minimum level of single-strandedness and a maximum probability of binding to existing 50-nucleotide oligomer concatemer sequences in the set, using NUPACK[35–37] to calculate these probabilities and a custom Python optimization script. PER concatemeric sequences were then subjected to a similar screening process (with Bowtie[52], Jellyfish[53] and BLAST[55]) as the 42-nucleotide oligomer bridge sequences (see above). See Supplementary Table 1 for a complete list of the probe primer sequences and hairpins used.

DNA synthesis and purification. Probes and bridge sequences were typically ordered unpurified (standard desalting) from IDT. The fluorescently labeled primer used in Fig. 1b, fluorescent imager oligonucleotides and many of the hairpins were HPLC purified. However, most primers can be successfully extended using unpurified hairpins bearing a 3′ poly(T) sequence, and probes for tissue FISH were generated in this manner. Oligonucleotides were pre-suspended in 1× TE buffer (10 mM Tris, 0.1 mM EDTA) at a 100-µM or 200-µM concentration and diluted in 1× TE to working concentrations of 10 µM. Stock and working solutions were stored at −20 °C. Complex oligonucleotide libraries for Figs. 4b and 6 were ordered from Twist Bioscience and prepared as previously described[15,31,56]. In brief, libraries were first amplified using emulsion PCR, followed by large-scale PCR and then in vitro transcription[15] to generate RNA complements of probes. Reverse transcription and subsequent digestion of RNA produced single-stranded DNA probe sets.

PER concatemerization. Typically, 100-µl reactions were prepared with final concentrations of 1× PBS, 10 mM $MgSO_4$, 400–1,000 U ml^{-1} of Bst LF polymerase (NEB, M0275L or McLab, BPL-300), 300–600 µM each of dATP, dCTP and dTTP (NEB, N0446S), 100 nM of Clean.G hairpin, 50 nM–1 µM of hairpin(s) and water to 90 µl (see Supplementary Fig. 1a for a visual representation). We previously reported this type of preliminary incubation with the Clean.G hairpin as a strategy to filter out a small amount of contaminant nucleotides that can halt the extension (see Supplementary Fig. 6 from ref. [30]). After incubation for 15 min at 37 °C, 10 µl of 10 µM primer was added and the reaction was incubated another 1–3 h with another 20 min at 80 °C to heat-inactivate the polymerase. PER extension solutions were directly diluted into ISH solutions or, in the case of the 17-color chromosome walk (Fig. 6) and tissue experiments, purified and concentrated using a MinElute kit (Qiagen, cat. no. 28004) with distilled-water elution to reduce volume and salt concentration from the reaction condition. We evaluated lengths of concatemers by diluting 1 µl of in vitro reaction with 19 µl of water. Samples were then run on 1% E-Gel EX agarose gels (Thermo Fisher, G402001) for 10 min alongside 1 kb Plus dsDNA Ladder (Invitrogen) to estimate length and imaged with the SYBR Gold channel on a Typhoon FLA 9000 scanner. See Supplementary Tables 1 and 3 for complete PER sequences and extension and purification conditions for each experiment, and the Supplementary Protocols for a step-by-step PER protocol.

FISH in fixed cell chambers. Eight-well chambers (Ibidi, cat. no. 80827) were seeded with MRC-5 cells and placed in a tissue culture incubator (37 °C with 5% CO_2). Samples were rinsed in 1× PBS, fixed in 1× PBS with 4% (wt/vol) paraformaldehyde solution for 10 min and then rinsed with 1× PBS. Chambers were then optionally stored at 4 °C for up to 2 weeks before continuing to the ISH step.

3D DNA ISH closely followed previous protocols[21,31,33,56]. After fixation, samples were rinsed in 1× PBS (1 min), permeabilized in 1× PBS with 0.5% (vol/vol) Triton X-100 (10 min), washed in 1× PBS with 0.1% (vol/vol) Tween-20 (1× PBSTw) (2 min), incubated in 0.1 N HCl (5 min) and washed in 2× SSC with 0.1% (vol/vol) Tween-20 (2× SSCT) (1 × 1 min, 1 × 2 min). Samples were incubated in 2× SSCT with 50% (vol/vol) formamide (5 min) and transferred to fresh 2× SSCT with 50% (vol/vol) formamide at 60 °C (at least 1 h), and wells were then loaded with 125 µl of ISH solution consisting of 2× SSCT, 50% (vol/vol) formamide, 10% (wt/vol) dextran sulfate, 400 ng µl^{-1} RNase A (Thermo Fisher, EN0531) and each PER extension at a final concentration of ~67 nM (1:15 dilution from 1 µM PER). After denaturation at 80 °C (3 min), samples were incubated overnight at 44 °C on a flat-block thermocycler (Eppendorf, Mastercycler Nexus).

RNA ISH was performed similarly to 3D DNA FISH, but with a shortened protocol. After fixation, samples were rinsed in 1× PBS (1 min), permeabilized in 1× PBS with 0.5% (vol/vol) Triton X-100 (10 min) and washed in 1× PBSTw (1 min). Samples were then transferred to 2× SSCT (1 min) before wells were loaded with 125 µl of ISH solution comprising 2× SSCT, 50% (vol/vol) formamide, 10% (wt/vol) dextran sulfate and PER extension at a final concentration of ~67 nM. After denaturation at 60 °C (3 min), chambers were incubated overnight at 42 °C on a flat-block thermocycler.

After (DNA or RNA) ISH, 200 µl prewarmed 2× SSCT (at 60 °C) was added, and the hybridization solution was aspirated. Samples were then washed in prewarmed 2× SSCT at 60 °C (4 × 5 min) and in 2× SSCT at room temperature (2 × 2 min). Samples going directly to fluorescent hybridization were then transferred to 1× PBS and washed (1 min and then fresh solution). Samples were optionally held at 4 °C (1–2 d) before being used for the branching or fluorescent hybridization protocol.

Samples with one round of branching were washed in 2× SSCT at room temperature (2 min) before wells were loaded with branch hybridization solutions consisting of 2× SSCT, 30% (vol/vol) formamide, 10% (wt/vol) dextran sulfate and PER extension at a final concentration of ~67 nM (1:15 dilution from 1 µM PER). Hybridization was performed at 37 °C for 1.5 h. Samples were then washed as before in 2× SSCT (4 × 5 min at 60 °C with prewarmed buffer and 2 × 2 min at room temperature). For iterative branching experiments, the branching and washing steps were performed repeatedly with slightly less stringent conditions: 30 °C for 1 h for hybridization, 55 °C for the heated washes and only one of the two SSCT washes at room temperature. After branching, samples were transferred to 1× PBS and washed (1 min and then fresh solution). Samples were then typically held at 4 °C overnight before fluorescent hybridization was performed. See the Supplementary Protocols for a note about choosing the right branch hybridization condition for a given set of sequences.

For fluorescent hybridization, samples were rinsed in 1× PBS and then wells were loaded with 125 µl of fluorescent hybridization solution consisting of 1× PBS and 1 µM fluorescent imager strands. Samples were incubated at 37 °C (1 h), washed in prewarmed 1× PBS at 37 °C (5 min and 2 × 2 min), rinsed with 1× PBS at room temperature and transferred to SlowFade Gold with DAPI (Thermo Fisher, S36939) for diffraction-limited imaging. See Supplementary Table 3 for additional details and the Supplementary Protocols for step-by-step instructions for performing RNA FISH in cells.

Metaphase DNA FISH. Human metaphase chromosome spreads on slides (Applied Genetics Laboratories, XX 46N or XY 46N) were denatured in 2× SSCT with 70% (vol/vol) formamide at 70 °C (90 s) and then transferred to ice-cold 70% (vol/vol) ethanol (5 min), to 90% (vol/vol) ethanol (5 min) and to 100%

ethanol (5 min). Slides were air-dried before 25 µl of ISH solution consisting of 2× SSCT, 50% (vol/vol) formamide, 10% (wt/vol) dextran sulfate, 400 ng µl^{-1} RNase A (Thermo Fisher, EN0531), probe pools with bridges at ~500 nM and PER extensions at a final concentration of 96 or 192 nM were added. The hybridization solution was sealed underneath a coverslip with rubber cement, and the slide was placed into a humidified chamber inside an air incubator at 45 °C overnight. After hybridization, samples were washed in 2× SSCT at 60 °C (15 min) and in 2× SSCT at room temperature (2 × 5 min).

For spectral imaging (Fig. 4b), slides were transferred to 1× PBS and then dried before 25 µl of fluorescent hybridization solution consisting of 1× PBS with 1 µM fluorescent imager strands was added. After the hybridization solution was covered with a coverslip, slides were put into a humidified chamber and incubated in an air incubator at 37 °C (1 h). Slides were then washed three times (1 × 15 min and 2 × 5 min) at 37 °C in prewarmed 1× PBS and dried. SlowFade Gold with DAPI (12 µl; Thermo Fisher, S36939) was added and sealed underneath a coverslip with nail polish before imaging.

For the metaphase walk (Fig. 6), slides were transferred to 1× PBS after the post-FISH washes and then dried. A flow chamber (~50 µl in volume) was constructed using a coverslip attached to the slide using double-sided tape to allow fluid exchange, and samples were rehydrated in 1× PBS. Each hybridization, consisting of 1× PBS with 10% (wt/vol) dextran sulfate and 1 µM fluorescent imager strands, was incubated at room temperature for 15 min. For combinatorial hybridizations with PER concatemers mapped to two colors, each fluorescent imager strand was included at 500 nM, retaining the 1 µM overall concentration. After washing with 200 µl (~4× flow through the chamber), SlowFade Gold with DAPI (Thermo Fisher, S36939) was added for diffraction-limited imaging. Between each fluorescent hybridization, previous imager strands were stripped with formamide: SlowFade was washed out with 200 µl of 1× PBS before stripping was performed by flowing a total of 1.6 ml of 1× PBSTw containing 60% (vol/vol) formamide through the chamber over the course of 15 min. After stripping, slides were washed with 200 µl of 1× PBS, allowed to sit for 2 min and washed twice more with a total of 400 µl of 1× PBS before adding the next fluorescent hybridization solution. The slide was stored overnight at 4 °C after the first six hybridizations before subsequent stripping and hybridization steps.

***Cas9* colocalization experiment.** HEK293T cells were transfected with plasmid PX458 (ref. [57]) (Addgene, cat. no. 48138) encoding Cas9 and GFP, 2A-linked and grown for 2 d before fixation (as below for retinas but for 10 min instead of 25 min). RNA FISH was performed as described above in eight-well chambers (Ibidi, cat. no. 80827) using the fixed HEK293T cells with two independent 18-oligonucleotide probe sets targeting the *Cas9* transcript followed by fluorescent hybridization and imaging. Fluorescent exchange was used to displace the fluorescent probes (at room temperature): samples were rinsed twice with 1× PBS (1 min each) followed by incubation with the formamide displacement buffer (1× PBSTw with 60% (vol/vol) formamide) for 15 min. After two additional 1-min rinses with 1× PBS and a 2-min incubation in 2× SSCT, branch hybridization was performed as above to map to the two new PER-concatemer sequences. This was followed by fluorescent hybridization (as above) with antibody incubation just before the last step of adding SlowFade Gold with DAPI (Thermo Fisher, S36939). Antibody incubation took place at room temperature as follows: 5 min in a blocking solution consisting of 1× PBSTw with 0.5% (wt/vol) BSA (Sigma, A8806), 30 min with chicken anti-GFP (Abcam) primary antibody, washes (3× 5 min) in 1× PBSTw, 30 min with anti-chicken-488 (Jackson) secondary antibody and washes (3× 5 min) in 1× PBSTw. In the second round of imaging, the same cell regions were identified and imaged, so that their signal morphologies could be directly compared.

Retinal histology. Neural retinas were dissected in 1× PBS and fixed for 25 min at room temperature in 4% formaldehyde solution (diluted in 1× PBS from 16% methanol-free formaldehyde solution (Thermo Scientific, cat. no. 28908)). For cryosectioning, retinas were transferred to a solution composed of 50% OCT and 15% sucrose in 0.5× PBS and frozen in an ethanol bath before long-term storage at −80 °C. Cryosections cut to 35 or 40 µm were adhered to poly-(D-lysine)-coated (Sigma, P6407) eight-well Ibidi chamber slides and dried. Before hybridization, sections were washed in PBSTw and then received a pretreatment consisting of a mild proteinase K exposure (NEB, P8107S; diluted to 1.5 µg ml^{-1} in PBS, 15-min incubation) followed by post-fixation (10 min in 4% formaldehyde) and acetic anhydride (Sigma, A6404) treatment (2.5 µl ml^{-1} in 0.1 M TEA, pH 8, 10-min incubation), two PBSTw washes and a ddH_2O wash, as described previously[40]. Sections were then incubated at 43 °C in a hybridization oven in hybridization wash (40% formamide, 2× SSC pH 7 and 1% Tween-20) for 30 min before addition of prewarmed probe and hybridization solution. Probe concentrations were determined by NanoDrop and probes were added to a final mass of 1 µg in each well (120-µl volume) in hybridization solution (40% formamide, 2× SSC, pH 7, 1% Tween-20 and 10% dextran sulfate (Sigma, D8906)). After overnight incubation (18–24 h), slides were washed in 40% formamide hybridization wash (2 × 30 min), in 25% formamide hybridization wash (2 × 45 min) and in 2× SSCT (0.1% Tween) (2 × 15 min). For branching, the 27*.27*.27*.28 branch was extended to a length of 500 nucleotides and incubated for at least 5 h in hybridization solution at 37 °C. Washes were performed as for the primary probe incubation with the temperature set to 37 °C.

For fluorescent detection, slides were washed three times in 1× PBSTw at room temperature and then transferred to 37 °C for hybridization and subsequent wash steps. Detection oligonucleotides were diluted to a concentration of 1 µM in a 1× PBS solution with 0.2% Tween-20 and 10% dextran sulfate. This solution was incubated with the sample for 2 h and the sample was then washed in 1× PBSTw (4 × 7 min). Imaging was performed in 80% glycerol mounting medium (80% glycerol, 1× PBS, 20 mM Tris, pH 8, and 2.5 mg ml^{-1} propyl gallate). For serial detections, fluorescent oligonucleotides were stripped with a solution of 50% formamide in 1× PBS at room temperature (3 × 5 min washes) and washed in 1× PBSTw (3 × 2-min). For DNase digestion of the primary probe, after the first detection and formamide stripping of imager oligonucleotides, samples were washed in 1× PBSTw (3 × 5-min), once in DNase I buffer (Sigma, cat. no. 04716728001) and then incubated in 40 U DNase I or 80 U Exonuclease I (NEB, M0293S), representing a 1:50 dilution of each enzyme in DNase I buffer, with a total volume of 200 µl. Samples were incubated for 30 min at 37 °C and then washed at room temperature three times in 1× PBS with 5 mM EDTA, fixed for 10 min in 4% formaldehyde in 1× PBS and washed three times in 1× PBSTw before proceeding with the second overnight probe hybridization.

For detection of DNA, retinas were treated as described for RNA FISH with the addition of a 5-min treatment in a solution containing 1 N HCl and 0.5 M NaCl, followed by a 15-min incubation at 80 °C in a solution of 50% formamide and 2× SSC on a preheated metal block before hybridization of the primary probe. For simultaneous detection of RNA and DNA, DNA denaturation and hybridization were conducted after RNA detection. RNase A (Thermo Fisher, EN0531) was added to the primary probe hybridization solution for DNA FISH at a concentration of 200 ng µl^{-1}.

We subsequently performed optimization experiments determining that most pretreatment steps were unnecessary and that several steps in the protocol could be performed more rapidly. The proteinase K, post-fixation and acetic anhydride steps were eliminated and sections were only washed in 1× PBSTw (3 × 5 min) before addition of the hybridization wash. For the methanol condition, sections were additionally dehydrated through a methanol/PBS gradient (20% increments), kept in 100% methanol for 20 min at room temperature and then rehydrated. Hybridization and fluorescence detection times were as indicated in the Supplementary Protocols. For the fluorescent detection buffer without dextran sulfate, the dextran sulfate was replaced with ddH_2O. For probe precipitation, the reaction mixture was combined with 2.5 volumes of 100% ethanol and 1/10 volume of 3 M sodium acetate (pH 5.2), frozen at −80 °C for 30 min, spun for 25 min at 16,000*g* at 4 °C and washed twice with 80% ethanol. After resuspension in ddH_2O, the concentration was determined by NanoDrop. One microgram of the resulting suspension was used in a final volume of 120 µl in the hybridization well, as with column-purified probes. See the Supplementary Protocols for step-by-step instructions for performing retinal RNA FISH.

Whole-mount retinal staining. Whole-mount staining was conducted with a similar protocol but with extended hybridization and wash times. The primary probe was incubated for 32 h, followed by washes in 40% formamide hybridization wash (2 × 45 min), 25% formamide hybridization wash (2 × 90 min) and 2× SSCTw (2 × 20 min). Hybridizations and washes were performed using 200-µl volumes, and 1.8 µg of *Grik1* probe (500-nucleotide length) was used. Fluorescent oligonucleotides were incubated for 8 h followed by washes in 1× PBSTw (0.2% Tween) (3 × 30 min). Retinas were flattened by four incisions before fixation and underwent the extended pretreatment as described above. Next, flattened retinas were transferred to an Ibidi chamber slide with the ganglion cell layer facing up. Retinas were held in place by the application of a nylon mesh (SEFAR-NITEX, 03-64/45) cut to size and laid over the retina. The corners of the mesh were glued to the corners of the well using White Gorilla Glue. Before this step, retinas were transferred to an OCT and sucrose solution (see above) to protect tissue from dessication while the mesh was overlaid and the glue was dried. Before application of the first hybridization solution, the OCT solution was washed away with washes in 1× PBS with 0.3% Triton X-100 (Sigma, T8787) (3 × 10 min) followed by washes in ddH_2O (2 × 30 s).

Reporter assay. Reporter sequences were derived from full or partial sequences of genes commonly expressed heterologously in mammals: *dCas9* (template: Addgene, cat. no. 60954), *lacZ*, *cre* and *luciferase* (see Supplementary Table 1 for a full list of sequences). Reporter mRNAs were designed to be within a size range of 1–1.6 kb and targetable by 22–24 primary probes. We used a reporter plasmid with a minimal TATA promoter (Stagia3; ref. [44]), replacing the GFPiAP insert of this plasmid with the described reporter sequences by plasmid digestion with Age1 and EcoRV followed by insertion of the reporter sequences in frame using Gibson assembly and transformation into DH5α. For reporter validation, a *Vsx2* (*Chx10*) enhancer[44] was inserted upstream of the TATA box in each reporter plasmid at the EcoRI site using Gibson assembly. For reporter screening, each of the six regions corresponding to open chromatin peaks was amplified using PCR with purified *Mus musculus* genomic DNA as the template. PCR products were inserted upstream at the EcoRI site of reporter plasmids. Retina DNase I hypersensitivity

data (Gene Expression Omnibus accession code GSM1014198) that are available through the ENCODE consortium[45] were accessed using the UCSC Genome Browser[50]. Reporters were electroporated into mouse pups via subretinal injection at P1 as described[46] with a Femtojet Express pressure injector (Eppendorf, cat. no. 920010521) and pulled-glass needles. Plasmids were introduced at a concentration of 500 ng μl^{-1} for each construct. For experiments with DNA FISH detection of the plasmid, the CRM-4 reporter plasmid was electroporated at a concentration of 1.5 μg μl^{-1}. pCAGGS-3×NLS-TagBFP was co-electroporated at a concentration of 200 ng μl^{-1} to enable identification of electroporated regions before sectioning. For plasmid DNA FISH, pENTR/pSM2(CMV) GFP plasmid (Addgene, cat. no. 19170) was used as the co-electroporation marker at a concentration of 100 ng μl^{-1}. This plasmid has little sequence similarity to the Stagia3 backbone and is minimally targeted by the probe set used for detection of Stagia3. For validation of CRM-1 and CRM-4 using a protein-based (GFP) reporter assay, these enhancer sequences were recloned into Stagia3.

Retina immunofluorescence and WGA counterstain. WGA conjugated to 405s (Biotium, cat. no. 29027) was diluted to a concentration of 10 μg ml^{-1} in 1× PBSTw, and samples were incubated for 1 h after each round of fluorescent oligonucleotide detection. Slides were washed in 1× PBSTw (2 × 5 min) after WGA application. Antibodies were applied after FISH detection. Slides were preincubated in block (5% HIDS, 0.3% Triton X-100 in 1× PBS) for 1 h. Anti-PKCα at 1:1,500 (Millipore Sigma, P4334) and anti-calretinin at 1:1,000 (Millipore Sigma, AB1550) were incubated overnight at 4 °C in block, washed four times in 1× PBSTx (PBS with 0.3% Triton X-100) over the course of 2 h, incubated for at least 4 h in secondary antibody (1:500) and then washed for 30 min in 1× PBSTx before addition of mounting medium and imaging. For GFP reporters, GFP signal was amplified with chicken anti-GFP (Abcam, AB13970) at 1:1,000. Secondary antibodies used were as follows: donkey anti-goat Alexa Fluor 647 (Jackson ImmunoResearch, cat. no. 705-605-147), donkey anti-chicken Alexa Fluor 488 (Jackson ImmunoResearch, cat. no. 703-545-155) and donkey anti-rabbit Alexa Fluor 488 (Jackson ImmunoResearch, cat. no. 711-545-152).

Microscopy. Imaging of iterative branching and *Cas9* colocalization samples was conducted on an inverted Zeiss Axio Observer Z1 using a 100× Plan-Apochromat oil objective with numerical aperture 1.40 and an LED light source. Samples were illuminated with a Colibri light source using a 365-nm, 470-nm, 555-nm or 625-nm LED. A filter set composed of a 365-nm cleanup filter (Zeiss, G 365), a 395-nm long-pass dichroic mirror (Zeiss, FT 395) and a 445/50-nm band-pass emission filter (Zeiss, BP 445/50) was used to visualize DAPI staining. A filter set composed of a 470/40-nm excitation filter (Zeiss, BP 470/40), a 495-nm long-pass dichroic mirror (Zeiss, FT 495) and a 525/50-nm band-pass emission filter (Zeiss, BP 525/50) was used to visualize ATTO 488 signal. A filter set composed of a 545/25-nm excitation filter (Zeiss, BP 545/25), a 570-nm long-pass dichroic mirror (Zeiss, FT 570) and a 605/70-nm band-pass emission filter (Zeiss, BP 605/70) was used to visualize ATTO 565 signal. Finally, a filter set composed of a 640/30-nm excitation filter (Zeiss, BP 640/30), a 660-nm long-pass dichroic mirror (Zeiss, FT 660) and a 690/50-nm band-pass emission filter (Zeiss, BP 690/50) was used to visualize Alexa Fluor 647 signal. Images were acquired with a Hamamatsu Orca-Flash 4.0 v3 sCMOS camera with 6.5-μm pixels, resulting in an effective magnified pixel size of 65 nm.

Remaining cell and metaphase samples were imaged on a Nikon Eclipse Ti-E microscope with a CFI Plan Apo 100× oil objective with numerical aperture 1.45 and an LED light source. Illumination was performed with a Spectra X LED system (Lumencor) using a 395/25-nm, 295-mW LED for DAPI signal, a 470/24-nm, 196-mW LED for ATTO 488 signal, a 550/15-nm, 260-mW LED for ATTO 565 signal and a 640/30-nm, 231-mW LED for Alexa Fluor 647 signal. Illumination light was spectrally filtered and directed to the objective, and emission light was spectrally filtered and directed to the camera by one of four filter cubes: (1) Semrock BFP-A-Basic-NTE for DAPI; (2) Semrock FITC-2024BNTE-ZERO for ATTO 488; (3) Semrock TRITC-B-NTE-0 for ATTO 565; and (4) Semrock Cy5-4040C-NTE-ZERO for Alexa Fluor 647 signal. An Andor Zyla 4.2 Plus sCMOS camera was used to acquire images with 6.5-μm pixels, resulting in an effective magnified pixel size of 65 nm.

All tissue images were acquired on a Zeiss Axio Observer Z1 inverted microscope equipped with an LSM780 single-point scanning confocal attachment containing two Quasar alkali photomultiplier modules and a GAaSP 32-channel spectral detector. Images were acquired using either a Plan Apo 40×/1.3-NA differential interference contrast or Plan Apo 63×/1.4-NA differential interference contrast oil objective. Laser lines used were 405 nm, 488 nm, 561 nm, 594 nm and 633 nm. Dichroic and main bean splitters used were MBS458, MBS488, MBS488/561/633, 405. The imaging software was ZEN Black 2012.

Image processing. Maximum projections taken on the Nikon Eclipse Ti-E microscope were processed using Nikon Elements software and by Zeiss ZEN software for non-confocal images taken on the Zeiss Axio Observer 1. Images were then processed with Fiji and ImageJ[58,59]. Multicolor overlays of cells and metaphase spreads were generated using Python scripts written to mimic the 'screen' behavior of Photoshop, which also allowed automatic cropping, contrasting and DAPI alignment. Most images presented in the main and supplementary figures utilized maximum projections of *z*-stacks, with the exception of the metaphase spread in Fig. 4b, the interphase image in Fig. 4b and the metaphase spreads in Fig. 6, for which single in-focus *z* slices for each hybridization were utilized to create overlays. For cell images with nuclei outlined, nuclear outlines were first automatically generated using CellProfiler[38,60] analysis pipelines (see below), and then these outlines were automatically added and re-styled in Adobe Illustrator. Scale bars were added in either Adobe InDesign or Adobe Illustrator on the basis of expected pixel size scaling. For retina images, maximum-intensity projections were generated in ZEN 2.3 lite. Multicolor overlays were generated using the screen setting in Adobe Photoshop, and brightness and contrast were adjusted for display purposes using Adobe Photoshop or Fiji and ImageJ[59]. For whole-mount volume visualizations, the ImageJ plugins '3D Viewer' and 'Volume Viewer' were used. For quantification of intensities and puncta detection in retina tissue, MATLAB and the Image Processing Toolbox were used (MATLAB and Image Processing Toolbox release R2018a, MathWorks). Open Microscopy Environment's Bio-Formats library[61] was used for manipulation of image files, including import of image stacks to the MATLAB environment.

In all cases except where otherwise noted in figure legends, images were only contrasted to improve signal visibility by changing the minimum (black) and maximum (white) values. Tissue autofluorescence was subtracted for Fig. 5d using puncta detection (see below) and background masking for each marker. High-resolution images of detected puncta (as shown in Fig. 7j) were generated by resizing puncta centroid images using bicubic interpolation and dilation on the basis of empirically estimated puncta size.

Quantification and statistical analysis. *Puncta quantification in cells.* Maximum-intensity projections in *z* were created using Nikon Elements software from raw mutlichannel *z*-stacks. These maximum projections were then inputted into CellProfiler 3.0 (refs. [38,60]), in which an automated image analysis pipeline was constructed to identify nuclei, cell bodies and FISH foci and to calculate the background-subtracted maximum pixel intensity of each segmented focus. For intensity-quantification experiments, the same pipeline was used for all conditions being compared. For cases where the number of puncta per cell or nucleus was calculated, a parent–child relationship was established between the FISH foci and the respective cellular or subcellular feature. For calculations of fold enhancement in Fig. 2b,d and Supplementary Fig. 3c, background was calculated as the mean of the image pixels masked for the detected puncta. Distributions of the background-subtracted peak intensity of puncta were then divided by the average of the corresponding distribution for the unextended condition. Cumulative density distributions depicted in Fig. 2g did not subtract background for calculations of fold enhancement because the sample was very crowded. In Fig. 4d, colocalization of puncta was assumed if any pixels within the detected area of a punctum in one channel overlapped with any pixels corresponding to a punctum detected in the other channel. See Supplementary Table 4, which contains cell counts, puncta counts and data for amplification, SNR, puncta counts per body and puncta area distributions.

Drop-seq data processing. Drop-seq data[40] for bipolar cells were processed according to the markdown accompanying the manuscript using class file class.R (https://github.com/broadinstitute/BipolarCell2016). All 10,888 cells identified to be present in cluster 1 (corresponding to rod bipolar cells) following Louvain clustering and cluster merging were used for plotting the average number of transcripts per cell. This analysis discards cells considered of poor quality with fewer than 500 detected genes per cell.

Retina image analysis. Serially detected retina images were aligned on the basis of the WGA stain using intensity-based image-registration algorithms in the MATLAB Image Processing Toolbox. Cells were segmented by application of the open-source membrane-based segmentation software ACME[41] to WGA images. For serial imaging, cell segmentation was performed on the WGA channel from a single session and applied to all registered channels. After automated segmentation, results were verified and visualized using ITK-SNAP[62].

Puncta were detected in 3D *z*-stack images using a Laplacian of Gaussian method[63], similar to the analogous two-dimensional pipeline implemented in ref. [5]. In brief, this involves convolving the original SABER image with a noise-suppressing elliptical Gaussian filter with a filter size corresponding to the empirical size of the imaged SABER puncta. The Laplacian of the Gaussian-filtered image was taken to enhance signal detection, and a threshold was set to identify puncta in a semiautomated way. See Supplementary Fig. 4c,d and below for details. Intensity quantification in tissue was done by puncta detection, taking the maximum pixel intensity of each punctum and subtracting the average background intensity for each image. We calculated the average intensity of background pixels by taking the average intensity of the image masked by the complement of a spherically dilated image of detected puncta centroids (radius = 2 μm). See Supplementary Table 4 for puncta and section numbers.

A universal threshold was applied to label cells as positive for each marker on the basis of the distribution of puncta per cell (see Supplementary Fig. 4e for details). Thresholds were 15, 5 and 2 for *Prkca*, *Tpbg* and *Slc4a*, respectively. For the quantification of reporter RNA versus plasmid DNA, a threshold of two puncta

per cell was used for CRM-4 reporter RNA, seven puncta per cell was used for endogenous *Grik1* and three puncta per cell was used for plasmid DNA.

To subtract tissue autofluorescence for the 9× retina overlay, puncta were first detected in 3D by the described method, and a Gaussian filter slightly larger than that used for puncta detection was convolved with the image of puncta centroids to capture all voxels in the puncta. The resulting mask was applied to the original SABER image, yielding a background-subtracted version of the original image while preserving the original signal pattern.

For high-resolution renderings of detected puncta (as shown in Fig. 7j), images of the centers of detected puncta were resized to a resolution of 10 nm per pixel using bicubic interpolation and then spherically dilated to a size similar to the original puncta, which can be estimated using the 'Measure' function (under the 'Analyze' menu in ImageJ) based on the original SABER images.

Reporter specificity analysis. The plasmid DNA FISH images were used to estimate that 52% of electroporated cells were rods, 9% were positive for *Grik1* endogenous RNA, 18% were ON bipolar cells, 12% were Müller glia and 9% were amacrine cells. These numbers were estimated directly from the data on the basis of plasmid DNA detection, *Grik1* mRNA expression and the known localization of cell bodies of each cell type. Reporter specificity was evaluated using a hypergeometric test[64] to define the probability of observing the empirical patterns of positive cells for each CRM. For a given CRM-driven reporter (CRM-1 to CRM-6) and endogenous gene (*Rho*, *Grm6*, *Grik1*, *Glyt1/Gad1*, other), we can consider C_{G^+} as the number of CRM-reporter-positive cells that are positive for the endogenous gene.

$$P(C_{G^+} \mid C, N, n) = \frac{\binom{n}{C_{G^+}}\binom{N-n}{C-C_{G^+}}}{\binom{N}{C}}$$

where $C_{G+} = |\mathrm{CRM}^+ \cap \mathrm{GENE}^+|$ is the total number of cells positive for both the CRM and gene; CRM^+ is the set of cells positive for CRM-driven reporter RNA; GENE^+ is the set of cells positive for endogenous gene; N is the total number of cells that received CRM-reporter plasmid DNA; n is the total number of GENE^+ in the plasmid-receiving population; and $C = |\mathrm{CRM}^+|$ is the total number of cells observed positive for CRM reporter RNA.

We took $N = 1{,}500$ as an estimate of the total cell population assayed for each CRM on the basis of the number of plasmid-positive cells observed in the DNA FISH experiment. In any one 240 µm × 240 µm electroporated retinal region, we estimate that approximately 300 cells received plasmid DNA, which is based on the automated cell segmentation. Cells were analyzed across five similar retinal regions, yielding a total population size of approximately 1,500 cells. With this estimate, n can be inferred on the basis of the proportion of each endogenous marker within the electroporated population. Both C and C_{G^+} were directly measured.

Statistics and reproducibility. All retina histology experiments were conducted at least twice on separate occasions with similar results. For figure displays, quantification was performed for at least three retinal sections from one animal from a single experiment with the exception of the distance plot in Fig. 5d, which is specific to the image shown. The exact number of biological replicates for all experiments is listed in Supplementary Table 4. Cell experiments were performed a number of times with similar results before the final data were quantified for a single experiment. Further internal controls, including quantitative comparison with sequencing data, colocalization of signal from independent probe sets, negative controls with probes or other elements missing, and signals matching expected morphologies, further increase our confidence in the consistency and reproducibility of the technique applied in multiple contexts.

Plotting and visualization. Most plots and some image overlays were generated in Python, using the Matplotlib[65], Seaborn[66], NumPy[67], Pandas[68], PIL and Biopython[69] libraries. Data were either imported in CSV format or read in from CellProfiler[38,60] output files. The plot in Fig. 7f was generated using the ggballoonplot function of ggpubr[70], a package for ggplot2 (ref. [71]) in R[72]. All box plots were generated using the default settings of Seaborn[66].

Reporting Summary. Further information on research design is available in the Nature Research Reporting Summary linked to this article.

Data availability

All raw and processed data are available from the authors upon reasonable request.

Code availability

The complete set of CellProfiler[38,60] pipelines used and example input images for each are available at https://github.com/brianbeliveau/SABER. PD3D, a package of MATLAB functions for detecting SABER puncta (or other fluorescent puncta) in 3D and assigning puncta to cells in a watershed segmentation, is available at https://github.com/ewest11/PD3D. Functions used for image processing are available at http://saber.fish or http://saber-fish.net/.

References

49. Yildirim, E., Sadreyev, R. I., Pinter, S. F. & Lee, J. T. X-chromosome hyperactivation in mammals via nonlinear relationships between chromatin states and transcription. *Nat. Struct. Mol. Biol.* **19**, 56–61 (2011).
50. Kent, W. J. et al. The Human Genome Browser at UCSC. *Genome Res.* **12**, 996–1006 (2002).
51. Quinlan, A. R. & Hall, I. M. BEDTools: a flexible suite of utilities for comparing genomic features. *Bioinformatics* **26**, 841–842 (2010).
52. Langmead, B. & Salzberg, S. L. Fast gapped-read alignment with Bowtie 2. *Nat. Methods* **9**, 357–359 (2012).
53. Marçais, G. & Kingsford, C. A fast, lock-free approach for efficient parallel counting of occurrences of *k*-mers. *Bioinformatics* **27**, 764–770 (2011).
54. Casanova, M. et al. Heterochromatin reorganization during early mouse development requires a single-stranded noncoding transcript. *Cell Rep.* **4**, 1156–1167 (2013).
55. Altschul, S. F., Gish, W., Miller, W., Myers, E. W. & Lipman, D. J. Basic local alignment search tool. *J. Mol. Biol.* **215**, 403–410 (1990).
56. Beliveau, B. J., Apostolopoulos, N. & Wu, C. Visualizing genomes with Oligopaint FISH probes. *Curr. Protoc. Mol. Biol.* **2014**, 14.23.1–14.23.20 (2014).
57. Ran, F. A. et al. Genome engineering using the CRISPR–Cas9 system. *Nat. Protoc.* **8**, 2281–2308 (2013).
58. Schneider, C. A., Rasband, W. S. & Eliceiri, K. W. NIH Image to ImageJ: 25 years of image analysis. *Nat. Methods* **9**, 671–675 (2012).
59. Schindelin, J. et al. Fiji: an open-source platform for biological-image analysis. *Nat. Methods* **9**, 676–682 (2012).
60. McQuin, C. et al. CellProfiler 3.0: next-generation image processing for biology. *PLoS Biol.* **16**, 1–17 (2018).
61. Linkert, M. et al. Metadata matters: access to image data in the real world. *J. Cell Biol.* **189**, 777–782 (2010).
62. Yushkevich, P. A. et al. User-guided 3D active contour segmentation of anatomical structures: significantly improved efficiency and reliability. *Neuroimage* **31**, 1116–1128 (2006).
63. Marr, D. & Hildreth, E. Theory of edge detection. *Proc. R. Soc. Lond. B Biol. Sci.* **207**, 187–217 (1980).
64. Plaisier, S., Taschereau, R., Wong, J. & Graeber, T. Rank-rank hypergeometric overlap: identification of statistically significant overlap between gene-expression signatures. *Nucleic Acids Res.* **38**, e169 (2010).
65. Hunter, J. D. Matplotlib: a 2D graphics environment. *Comput. Sci. Eng.* **9**, 90–95 (2007).
66. Waskom, M. et al. mwaskom/seaborn: v0.8.1. https://doi.org/10.5281/zenodo.883859 (2017).
67. Oliphant, T. E. *A Guide to NumPy* (Trelgol Publishing, 2006).
68. McKinney, W. Data structures for statistical computing in Python. in *Proc. 9th Python in Science Conference* (eds. van der Walt, S. & Millman, J.) 51–56 (SciPy, 2010).
69. Cock, P. J. A. et al. Biopython: freely available Python tools for computational molecular biology and bioinformatics. *Bioinformatics* **25**, 1422–1423 (2009).
70. Kassambara, A. ggpubr: 'ggplot2' based publication ready plots, version 0.1.7. https://cran.r-project.org/web/packages/ggpubr/index.html (2018).
71. Wickham, H. *ggplot2: Elegant Graphics for Data Analysis* (Springer, 2016).
72. R Core Team. *R: A Language and Environment for Statistical Computing* (R Foundation for Statistical Computing, 2013).

nature research

Corresponding author(s): Dr. Peng Yin, Dr. Constance Cepko, Dr. Brian Beliveau

Last updated by author(s): 4/25/2019

Reporting Summary

Nature Research wishes to improve the reproducibility of the work that we publish. This form provides structure for consistency and transparency in reporting. For further information on Nature Research policies, see Authors & Referees and the Editorial Policy Checklist.

Statistics

For all statistical analyses, confirm that the following items are present in the figure legend, table legend, main text, or Methods section.

n/a	Confirmed	
☐	☒	The exact sample size (*n*) for each experimental group/condition, given as a discrete number and unit of measurement
☐	☒	A statement on whether measurements were taken from distinct samples or whether the same sample was measured repeatedly
☐	☒	The statistical test(s) used AND whether they are one- or two-sided *Only common tests should be described solely by name; describe more complex techniques in the Methods section.*
☒	☐	A description of all covariates tested
☐	☒	A description of any assumptions or corrections, such as tests of normality and adjustment for multiple comparisons
☐	☒	A full description of the statistical parameters including central tendency (e.g. means) or other basic estimates (e.g. regression coefficient) AND variation (e.g. standard deviation) or associated estimates of uncertainty (e.g. confidence intervals)
☐	☒	For null hypothesis testing, the test statistic (e.g. *F*, *t*, *r*) with confidence intervals, effect sizes, degrees of freedom and *P* value noted *Give P values as exact values whenever suitable.*
☒	☐	For Bayesian analysis, information on the choice of priors and Markov chain Monte Carlo settings
☒	☐	For hierarchical and complex designs, identification of the appropriate level for tests and full reporting of outcomes
☐	☒	Estimates of effect sizes (e.g. Cohen's *d*, Pearson's *r*), indicating how they were calculated

Our web collection on statistics for biologists contains articles on many of the points above.

Software and code

Policy information about availability of computer code

Data collection	Nikon Elements (NIS ElementsAR ver. 4.6.0.) and Zeiss Zen software (2012 S4) were used to acquire images.
Data analysis	ImageJ2/FIJI, Photoshop ('screen') overlay method, or custom Python code were used to contrast and overlay images as described in the Methods section. NUPACK 3.0.4 was used to calculate cross-hybridization probabilities of PER concatamers and Bowtie2: 2.2.4 Jellyfish 2.2.4, and BLASTn (https://blast.ncbi.nlm.nih.gov/Blast.cgi) were used to further process sequences. Puncta were identified and assigned to single cells using CellProfiler 3.0 or custom MATLAB (version 2018a) pipelines (PD3D - all now available online). Cell segmentation was performed with previously published software (ACME: https://wiki.med.harvard.edu/SysBio/Megason/ACME), and plots were generated with Python (version 2.7) and Seaborn (version 0.8.1) or in R (version 3.5.1).

For manuscripts utilizing custom algorithms or software that are central to the research but not yet described in published literature, software must be made available to editors/reviewers. We strongly encourage code deposition in a community repository (e.g. GitHub). See the Nature Research guidelines for submitting code & software for further information.

Data

Policy information about availability of data

All manuscripts must include a data availability statement. This statement should provide the following information, where applicable:

- Accession codes, unique identifiers, or web links for publicly available datasets
- A list of figures that have associated raw data
- A description of any restrictions on data availability

All raw and processed data will be made available upon request.

Field-specific reporting

Please select the one below that is the best fit for your research. If you are not sure, read the appropriate sections before making your selection.

☒ Life sciences ☐ Behavioural & social sciences ☐ Ecological, evolutionary & environmental sciences

For a reference copy of the document with all sections, see nature.com/documents/nr-reporting-summary-flat.pdf

Life sciences study design

All studies must disclose on these points even when the disclosure is negative.

Sample size	For experiments involving quantification of puncta, puncta intensity, and numbers of signal positive cells in retina, n=3 was chosen as the minimal replicate number, and sample size was determined by the number positive cells or puncta within the replicates. We determined this to be sufficient owing to internal control (specific staining of positionally defined cell types using known markers) and low observed variability between stained samples.
Data exclusions	Data were not excluded from analysis.
Replication	All replication attempts were successful and observed marker expression patterns were consistent with orthogonal methods and previously known results. For retinal probes used in this study, we find that in all cases the expression patterns were consistent with cell type-specific expectations from previous studies of RNA sequencing, as well as protein antibody stains. For final quantification, all samples were quantified for a minimum of three retinal sections with the exception of Figure 5D, where quantification of cell localizations are specific to the image shown.
Randomization	Retinas and sections used for imaging were selected randomly, however all cells and puncta that passed quality control were analyzed equally with no sub-sampling and thus, there was no requirement for randomization.
Blinding	Blinding was not possible as experimental conditions were evident from the image data. Quantifications were performed using computational pipeline applied equally to all conditions and replicates for a given probe. Thresholds for detecting puncta were chosen for each probe based on graphs with objective properties that appeared indistinguishable across conditions.

Reporting for specific materials, systems and methods

We require information from authors about some types of materials, experimental systems and methods used in many studies. Here, indicate whether each material, system or method listed is relevant to your study. If you are not sure if a list item applies to your research, read the appropriate section before selecting a response.

Materials & experimental systems

n/a	Involved in the study
☐	☒ Antibodies
☐	☒ Eukaryotic cell lines
☒	☐ Palaeontology
☐	☒ Animals and other organisms
☒	☐ Human research participants
☒	☐ Clinical data

Methods

n/a	Involved in the study
☒	☐ ChIP-seq
☒	☐ Flow cytometry
☒	☐ MRI-based neuroimaging

Antibodies

Antibodies used	Anti-PKCa (MilliporeSigma P4334, lot #085H4848), used at 1:1500 Anti-Calretinin (MilliporeSigma AB1550, lot #2510177), used at 1:1000 Anti-GFP (Abcam AB13970), used at 1:750 Donkey anti-Chicken Alexa488 (Jackson ImmunoResearch Laboratories, 703-545-155), used at 1:500 from 0.625mg/mL stock solution Donkey anti-Goat Alexa647 (Jackson ImmunoResearch Laboratories, 705-605-147), used at 1:500 from 0.625mg/mL stock solution Donkey anti-Rabbit Alexa488 (Jackson ImmunoResearch Laboratories, 711-545-152), used at 1:500 from 0.625mg/mL stock solution
Validation	Anti-PKCa (MilliporeSigma P4334) antibody has been validated by MilliporeSigma by demonstrating immunoblotting on rat brain extract and inhibition of this signal with an immunizing peptide (see website). This antibody was also validated in our previous work (Shekhar and Lapan, 2016), where it was shown to specifically label rod bipolar cells based on overlap with rod bipolar cell-specific markers that were identified in Drop-seq data.

Anti-Calretinin (MilliporeSigma AB1550) has been validated for use in immunohistochemistry and western blotting, as stated on the MilliporeSigma product page.

Eukaryotic cell lines

Policy information about cell lines

Cell line source(s)	MRC-5 (human, ATCC CCL-171) HEK293T cells (human, ATCC CRL-1573) EY.T4 cells (human, from J. T. Lee lab, see ref. 49)
Authentication	None of the cell lines have been authenticated.
Mycoplasma contamination	Cell lines were not tested for mycoplasma contamination but no indication of contamination was observed.
Commonly misidentified lines (See ICLAC register)	No commonly misidentified cell lines were used.

Animals and other organisms

Policy information about studies involving animals; ARRIVE guidelines recommended for reporting animal research

Laboratory animals	Wild-type CD1 mice (male and female) age P13, P17 or P25 were used for retina harvest.
Wild animals	No wild animals were used in this study.
Field-collected samples	No field-collected samples were used in this study.
Ethics oversight	The mouse work was performed under the study protocol IS00001679, as approved by the Institutional Animal Care and Use Committee.

Note that full information on the approval of the study protocol must also be provided in the manuscript.